SJER Scientific Journal of Engineering Research

futuristech PT. Teknologi Futuristik Indonesia

Date of publication February 11, 2026, date of current version February 11, 2026.
e-ISSN: 3109-1725
Digital Object Identifier 10.64539/sjer.v2i1.2026.372

Article

Real-Time Implementation of Integrated Optical Plus Filtered OFDM 5G Network Parameters for LTE and DVB-T2 Telecommunication Systems

Fatai Ahmed-Ade[1], Vincent Andrew Akpan[2,*], Emmanuel Omonigho Ogolo[3]

[1] Department of Physics, Federal University of Lokoja, P.M.B. 1154, Lokoja, Kogi State, Nigeria; ahmedadefatai@gmail.com
[2] Department of Biomedical Engineering, The Federal University of Technology, P.M.B. 704 Akure, Nigeria; vaakpan@futa.edu.ng
[3] Department of Physics, The Federal University of Technology, P.M.B 704 Akure, Ondo State, Nigeria; eoogolo@futa.edu.ng
* Correspondence

This work was supported by Institute Based Research grant from the Tertiary Education Trust Fund (TETFund), Federal Government of Nigeria.

Abstract: Orthogonal Frequency Division Multiplexing (OFDM) technology to deliver mobile broadband and digital television services. This paper presents the real-time implementation of Optical plus Filtered OFDM (O+F OFDM) algorithms for Long Term Evolution (LTE) mobile networks and Digital Video Broadcasting – Second Generation Terrestrial (DVB-T2) systems, with particular focus on deployments in emerging markets. The paper analyzes physical-layer configurations specified in 3GPP TS 36.211 and ETSI EN 302 755, including subcarrier spacing, Fast Fourier Transform (FFT) sizes, cyclic prefix options, modulation schemes, and Multiple-Input Multiple-Output (MIMO) configurations. Field measurements from Nigerian LTE deployments reveal that while theoretical peak rates approach 300 Mbps with 4×4 MIMO on 20 MHz carriers, achieved throughput typically ranges from 15-35 Mbps due to backhaul constraints, interference, and suboptimal network configuration. For DVB-T2, we document parameters enabling 30-50% greater spectral efficiency than first-generation standards through enhanced forward error correction, larger FFT options (up to 32k subcarriers), and rotated constellations. The O+F OFDM implementation demonstrates superior performance characteristics: reduced out-of-band emissions (>45 dB suppression), improved spectral confinement within regulatory masks, and enhanced multipath resilience through optical filtering stages. System-level considerations including adaptive modulation and coding, Quality-of-Service (QoS) bearer management, Self-Organizing Network (SON) algorithms, and carrier aggregation are examined. We strongly recommend Field-Programmable Gate Array (FPGA)-based real-time implementation of O+F OFDM for both MTN's LTE and GOtv's DVB-T2 systems to achieve deterministic signal processing latency below 5 microseconds, support adaptive parameter reconfiguration without hardware modifications, and enable power-efficient operation critical for Nigerian deployment scenarios with unreliable electrical infrastructure.

Keywords: DVB-T2; Real-Time Implementation; GOtv; LTE; MTN Nigeria; Network Optimization; Optical+Filtered OFDM; Quality of Service (QoS).

1. Introduction

The telecommunications sector has undergone profound transformation over the past fifteen years, evolving from basic voice services into complex ecosystems delivering high-definition video, real-time interactive applications, telemedicine, and mobile financial services to billions of users worldwide [1]-[3]. This evolution has been driven by insatiable demand for bandwidth-intensive ap-

Table 1. List of abbreviations and meaning.

S/N	Abbreviations	Meaning	S/N	Abbreviations	Meaning
1	OFDM	Orthogonal Frequency Division Multiplexing	37	IMT-2030	International Mobile Telecommunication-2030
2	LTE	Long Term Evolution	38	UE	User Equipment
3	ESTI EN	European Cybersecurity Standards for Internet of Things	39	E-UTRAN	Evolved Universal Terrestrial Radio Access Network
4	ETSI	European telecommunication Standard Institute	40	FFT	Fast Fourier Transform
5	ITU-R	International Telecommunication Union Radiocommunication Sector	41	DVB-T2	Digital Video Broadcasting – Second Generation Terrestrial
6	MIMO	Multiple Input Multiple Output	42	3G	Third Generation
7	QoS	Quality-of-Service	43	5G	Fifth Generation
8	SON	Self-Organizing Network	44	6G	Sixth Generation
9	FPGA	Field Programmable Gate Array	45	AWGN	Additive white Gaussian noise
10	MTN	Mobile Telecommunication Network	46	PLP	Physical Layer Pipes
11	SINR	Signal-to-Interference-plus-Noise Ratio	47	EPS	Evolved Packet System
12	BCH	Bose-Chaudhuri-Hocquenghem	48	dB	Decibel
13	FDMA	Frequency division multiple access	49	MAC	Media access control
14	ICIC	Inter-cell interference coordination	50	CP	Cyclic prefix
15	QAM	Quadrature amplitude modulation	51	GBR	Guaranteed Bit Rate
16	LDPC	Low-Density Parity-Check	52	KPI	Key Performance Indicator
17	SFN	Single Frequency Network	53	IP	Internet protocol
18	3GPP	Third Generation Partnership Project	54	D-SON	Distributed SON
19	ITU	International Telecommunication Union	55	PCI	Physical Cell ID
20	RSRP	Reference Signal Received Power	56	CA	Carrier Aggregation
21	RSRQ	Reference Signal Received Quality	57	MHz	Mega Hertz
22	HARQ	Hybrid Automatic Repeat Request	58	UHF	Ultra High Frequency
23	AMC	Adaptive Modulation and Coding	59	SC-FDMA	Single Carrier FDMA
24	PCRF	Policy and Charging Rules Function	60	eICIC	enhanced ICIC
25	QPSK	Quadrature phase shift keying	61	ABS	Almost Blank Subframes
26	E1	European format for digital transmission	62	DSP	Digital Signal Processors
27	RAN	Radio Access Network	63	GPU	Graphics Processing Units
28	C/N	Carrier-to-Noise Ratio	64	GPS	Global positioning system
29	O+F OFDM	Optical Plus Filtered OFDM	65	GI	Gateway interface
30	FEC	Forward error correction	66	TS	Technical specification
31	RB	Resource Block	67	RNG	Random number generator
32	QCI	QoS Class Identifiers	68	MER	Modulation Error Ratio
33	CBRS	Citizens Broadband Radio Service	69	LSA	Licensed Shared Access
34	IFFT	Inverse Fast Fourier Transform	70	CQI	Channel Quality Indicator
35	PSD	Power Spectral Density	71	TU6	Typical Urban 6-Path Channel Model
36	NCC	Nigerian Communications Commission	72	EVM	Error Vector Magnitude

plications, competitive pressures among service providers, regulatory mandates for spectrum efficiency, and breakthroughs in physical-layer technologies particularly OFDM and MIMO antenna systems [4], [5].

The transition from third-generation (3G) networks to Long Term Evolution (LTE) and subsequently to fifth-generation (5G) systems represents not merely incremental improvements in data rates but fundamental reconceptualization of wireless network architecture [6]. The 6th Generation (6G) network is the next evolution in mobile communication technology, expected to be commercially deployed around 2030 [7], [8]. It aims to extend and surpass

Table 2. LTE OFDM Physical-Layer Parameters from 3GPP TS 36.211.

S/N	Channel BW (MHz)	FFT Size	Usable Subcarriers	Resource Blocks	Sampling Rate (MHz)
1	1.4	128	72	6	1.92
2	3	265	180	15	3.84
3	5	512	300	25	7.68
4	10	1024	600	50	15.36
5	15	1536	900	75	23.04
6	20	2048	1200	100	30.72

Table 3. LTE MIMO Configurations and Peak Downlink Rates (from 3GPP specifications and field trial data).

S/N	MIMO Configuration	Antenna Setup	Spatial Streams	Peak Rate (20 MHz, 64-QAM, code rate 0.9)
1	2×2	2 Tx, 2 Rx	Up to 2	~150 Mbps
2	4×2	4 Tx, 2 Rx	Up to 2	~150 Mbps
3	4×4	4 Tx, 4 Rx	Up to 4	~300 Mbps
4	8×8	8 Tx, 8 Rx	Up to 8	~600 Mbps

Table 4. DVB-T2 FFT Sizes and Guard Interval Options from ETSI and ITU-R.

S/N	FFT Size	Sub-carriers	Guard Interval Fractions	Typical Application
1	1k	1024	1/128, 1/32, 1/16, 1/8, 1/4	Small non-SFN networks
2	2k	2048	1/128, 1/32, 1/16, 1/8, 1/4	Moderate coverage
3	4k	4096	1/128, 1/32, 1/16, 1/8, 1/4	Regional networks
4	8k	8192	1/128, 1/32, 1/16, 1/8, 1/4, 19/128, 19/256	Standard SFN
5	16k	16384	1/128, 1/32, 1/16, 1/8, 1/4, 19/128, 19/256	Large SFN
6	32k	32768	1/128, 1/32, 1/16, 1/8, 1/4, 19/128, 19/256	Very large SFN (>60 km)

5G in speed, reliability, intelligence, and connectivity density, enabling a fully digital, intelligent, and immersive world. The International Telecommunication Union (ITU) has established the International Mobile Telecommunication-2030 (IMT-2030) framework to guide the development and standardization of 6G technologies [7], [8].

LTE, standardized by the 3rd Generation Partnership Project (3GPP), employs OFDMA for the downlink and Single Carrier FDMA (SC-FDMA) for the uplink, achieving peak downlink rates exceeding 300 Mbps with advanced MIMO configurations [4]. The integration of Optical plus Filtered OFDM (O+F OFDM) techniques, as demonstrated by Ahmed-Ade and co-workers [9], [10], provides enhanced spectral confinement and reduced interference compared to conventional OFDM implementations. Quadrature amplitude modulation (QAM) is a digital modulation scheme that transmits data by varying both the amplitude and phase of a carrier signal, enabling efficient spectral utilization. Similarly, Digital Video Broadcasting-Second Generation Terrestrial (DVB-T2), standardized by the European Telecommunications Standards Institute (ETSI), has revolutionized broadcast media delivery through sophisticated physical-layer enhancements including Low-Density Parity-Check (LDPC) coding, larger FFT sizes enabling extensive Single Frequency Networks (SFNs), and flexible modulation up to 256-QAM [11], [12].

Yet the march toward ubiquitous, high-quality connectivity has been neither smooth nor uniform [13]. Operators in emerging markets face daunting challenges: limited spectrum allocations, inadequate backhaul infrastructure, inconsistent power supply, and capital constraints that hinder network densification [14], [15]. In order to achieve consistent QoS, the set of performance attributes that must be satisfied include but not limited to throughput, latency, jitter, and packet loss that determine user satisfaction-remains elusive, particularly during peak demand periods or in environments with challenging radio propagation characteristics [16], [17].

This paper provides technical rigorous treatment of OFDM-based telecommunications systems with three principal objectives. Firstly, we clarify the conceptual and technical foundations of modern telecom systems, examining the architectural components and fundamental principles governing signal transmission, channel modeling, and capacity bounds. Secondly, we critically examine factors constraining QoS: spectrum scarcity, signal propagation impairments, backhaul limitations, configuration complexity, and traffic dynamics alongside technological innovations and operational measures introduced since 2010 to mitigate these limitations. Thirdly, we present detailed, standards-compliant OFDM implementation parameters for two representative deployment scenarios from the Nigerian telecommunication systems, namely: *1).*

LTE for 5G mobile cellular networks (exemplified by MTN operations in Nigeria and analogous markets) [18], [19]; and *2).* DVB-T2 terrestrial television (exemplified by MultiChoice's GOtv platform deployed across sub-Saharan Africa) [20]. This parameter sets, grounded in 3GPP [21] and ETSI [12] specifications and informed by field measurement studies; serve as actionable reference material for network planning, optimization, and troubleshooting. Additionally, we justify FPGA-based real-time implementation for both systems, demonstrating how reconfigurable hardware acceleration addresses the computational intensity of OFDM processing while providing flexibility for adaptive parameter optimization. All the abbreviations used in this paper and their respective meaning are listed in Table 1.

Optical Orthogonal Frequency Division Multiplexing (O-OFDM) is highly effective for high-speed transmission in both LTE (as part of radio-over-fiber) and DVB-T2 (for broadcasting infrastructure) due to its robustness against dispersive channels. However, the technique faces several critical challenges, primarily related to the high dynamic range of the signals and the inherent nature of optical components [9], [10]. The main problems of O-OFDM include but not limited to high peak-to-average power ratio (PAPR), sensitivity to optical nonlinearities, intensity modulation/direct detection (IM/DD) constraints, synchronization and frequency offset, and complex digital signal processing (DSP) [9], [10], [18]–[20]. On the other hand, filtered OFDM (f-OFDM) has been proposed to mitigate the high out-of-band (OOB) emissions and spectral leakage associated with the rectangular pulse shaping in conventional cyclic prefix OFDM (CP-OFDM) used in LTE and DVB-T2 [9], [10]. Furthermore, while F-OFDM improves spectral containment, it introduces several key problems and trade-offs in implementation and performance. The notable primary problems includes but not limited to increased system complexity and cost, intrinsic in-band interference, higher PAPR, filter tail issue, power inequality in subcarriers, and sensitivity to carrier frequency offset (CFO) [9], [10], [18]–[20].

Optical plus filtered OFDM (O+F OFDM) provides superior spectral efficiency, lower Signal-to-Noise Ratio (SNR) requirements (approx. 22.7 dB vs. 25.0 dB for conventional), and reduced nonlinear distortion by combining PAPR control with enhanced spectral shaping [9], [10]. O+F OFDM outperforms traditional O-OFDM and F-OFDM by optimizing bandwidth in 5G/6G, LTE, and DVB-T2 systems through tighter subcarrier packing and reduced out-of-band (OOB) emissions [9], [10]. This paper presents the real-time implementation of integrated O+F OFDM for evaluation of LTE and DVB-T2 on MTN Nigeria (mobile communication) and GOtv Nigeria (digital video broadcasting) telecommunication systems.

The paper is organized as follows. Section 2 presents a complete background knowledge required to understand the techniques presented in this paper. The detailed MTN Nigeria LTE and GOtv Nigeria DVB-T2 parameters and data required for the real-time implementation of the two scenarios are presented in Section 3. Section 4 provides a comprehensive algorithm design, methodology and real-time implementation strategies for the LTE and DVB-T2 based on O+F OFDM. The real-time Implementation results are presented in Section 5 together with detailed and extensive discussion of the results as well as their implications. Section 6 concludes the paper with directions on future works with particular emphasis on dedicated hardware realization.

2. Background Knowledge

2.1. LTE and DVB-T2 Standard Framework with ITU Recommendations

2.1.1. Standard Analysis Framework

The analysis presented in this paper synthesizes authoritative technical specifications from three primary standardization bodies, namely: *1).* 3GPP for LTE/LTE-Advanced (specifically technical specification (TS) 36.211 covering physical channels and modulation [4], [22]; TS 23.203 for policy and charging architecture [23]; and TS 36.300 for overall evolved universal terrestrial radio access network (E-UTRAN) description [24]); *2).* ETSI for DVB-T2 (EN 302 755 specifying frame structure, channel coding, and modulation [12]); and *3).* International Telecommunication Union (ITU) recommendations for frequency planning and propagation modeling (particularly International Telecommunication Union – Radiocommunication (ITU-R) Sector Report BT.2254 for DVB-T2 network planning [25] and the ITU-R P.1546-6 for propagation prediction [26].

2.1.2. Field Measurement Data Integration

This work incorporates empirical data from published field studies of LTE deployments in Nigeria, focusing on comparative performance measurements across multiple operators (MTN, Airtel, Glo, 9Mobile) conducted during 2019-2021 [19], [26], [27]. These studies employed drive testing methodologies with GPS-synchronized measurement equipment logging Reference Signal Received Power (RSRP), Reference Signal Received Quality (RSRQ), throughput, latency, and packet loss across diverse environments (urban, suburban, rural). Additionally, this work references DVB-T2 deployment reports from MultiChoice's GOtv operations in Nigeria, Kenya, Uganda, and South Africa documenting coverage achievements, modulation and coding configurations, and SFN implementations [20].

2.1.3. Parameter Extraction and Tabulation

For each technology (LTE and DVB-T2), we extract canonical physical-layer parameters from specifications,

Table 5. DVB-T2 Modulation and carrier-to-noise ratio (C/N) Requirements from ETSI EN 302 755 field measurements.

S/N	Modulation	Bits/ Symbol	Typical Code Rate	Required C/N (AWGN, dB)	Applications
1	QPSK	2	1/2	~3.5	Coverage extension, mobile
2	16-QAM	4	2/3	~11	Balanced coverage/capacity
3	64-QAM	6	3/4	~17	Fixed reception, good signal
4	256-QAM	8	3/4	~23	Fixed reception, strong signal

organizing them into systematic tables covering: *1).* OFDM waveform characteristics (subcarrier spacing, FFT sizes, cyclic prefix options); *2).* modulation and coding schemes with applicable signal-to-noise ratio requirements; *3).* MIMO configurations and expected throughput gains; and *4).* channel bandwidth allocations with corresponding resource block mappings. System-level parameters governing network operation QoS class identifiers, hybrid automatic repeat request (HARQ) configurations, power control algorithms, scheduling policies, and SON functions—are documented based on 3GPP specifications and operational best practices reported in peer-reviewed literature [28]-[31].

2.1.4. Performance Analysis Approach

The current work employs link budget calculations following standard methodologies [32] to relate physical-layer parameters (transmit power, antenna gains, modulation order) to coverage and capacity outcomes. For LTE, we calculate theoretical peak data rates using the formula:

$$Peak\ Rate = RBs \times \left.\begin{aligned} & \frac{12\ subcarriers}{RB} \times \frac{symbols}{slot} \\ & \times \frac{bits}{symbol} \times \frac{slots}{subframe} \\ & \times \frac{subframe}{s} \times MIMO\ layers \\ & \times code\ rate \end{aligned}\right\} \quad (1)$$

where the parameters are drawn from Table 1 configurations. For DVB-T2, we compute payload data rates accounting for FFT size, guard interval overhead, pilot overhead, forward error correction (FEC) code rate, and modulation order per ETSI specifications [12]. Field measurement data [26] is compared against these theoretical calculations to quantify the performance gap attributable to real-world impairments.

2.2. OFDM Physical-Layer Parameters

2.2.1. LTE Downlink Configuration

For the LTE downlink configuration, each Resource Block (RB) comprises 12 consecutive subcarriers in frequency and one 0.5 ms slot in time. The usable bandwidth is less than nominal channel bandwidth due to guard bands preventing adjacent-channel interference [33]. LTE defines two cyclic prefix (CP) configurations: Normal CP with seven OFDM symbols per slot (CP durations ~5.2 µs first symbol, ~4.7 µs remaining symbols) and Extended CP with six symbols per slot (uniform ~16.7 µs CP) [22]. Normal CP suffices for typical urban and suburban environments where delay spread rarely exceeds 5 µs; Extended CP addresses scenarios with high delay spread (large rural cells, SFN broadcast services). LTE employs OFDMA with fixed 15 kHz subcarrier spacing [4], [22]. The relationship between channel bandwidth and FFT size is precisely defined in 3GPP TS 36.211, as shown in Table 2.

The supported modulation schemes include quadrature phase shift keying (QPSK), 16-QAM, and 64-QAM as baseline, with 256-QAM introduced in LTE-Advanced Pro (Release 12+) for downlink under favorable link conditions requiring Signal-to-Interference-plus-Noise Ratio (SINR) exceeding 22 decibels (dB) [34]. Adaptive Modulation and Coding (AMC) dynamically selects modulation order and turbo code rate (ranging from ~1/3 to 0.9) based on Channel Quality Indicator (CQI) feedback from user equipment [35]. Table 3 summarizes MIMO configurations and theoretical peak rates [4], [36], [37].

However, a typical 8 x 8 MIMO system is rarely deployed due to limited User Equipment (UE) support and diminishing returns in typical propagation environments. Thus, UE refers to mobile devices (smart phones, tablets, modems) that connects to cellular networks as detailed in 3GPP specifications and field trial data [1], [15], [17].

Field measurements in Nigerian LTE networks reveal substantial gaps between theoretical and achieved performance [38]. A 2021 comparative study documented average downlink throughput of 15-35 Mbps for MTN (the market leader with broader spectrum holdings and denser deployment) and 5-15 Mbps for competitors with narrower bandwidths and sparser sites [26]. Median latencies ranged from 40-80 ms, significantly exceeding theoretical LTE minimums (~10 ms), attributed to backhaul congestion and core network delays. During congestion, latencies exceeded 200 ms and packet loss spiked to 5-10%, severely degrading interactive applications [26].

2.2.2. DVB-T2 Physical-Layer Configuration

DVB-T2 supports seven FFT sizes (1k to 32k) enabling flexible deployment strategies [39]. Larger FFTs facilitate extensive SFNs where multiple synchronized transmitters broadcast identical signals, with receivers combining delayed replicas provided delays fall within the guard interval [20], [30]. Table 4 presents DVB-T2 FFT and guard in-

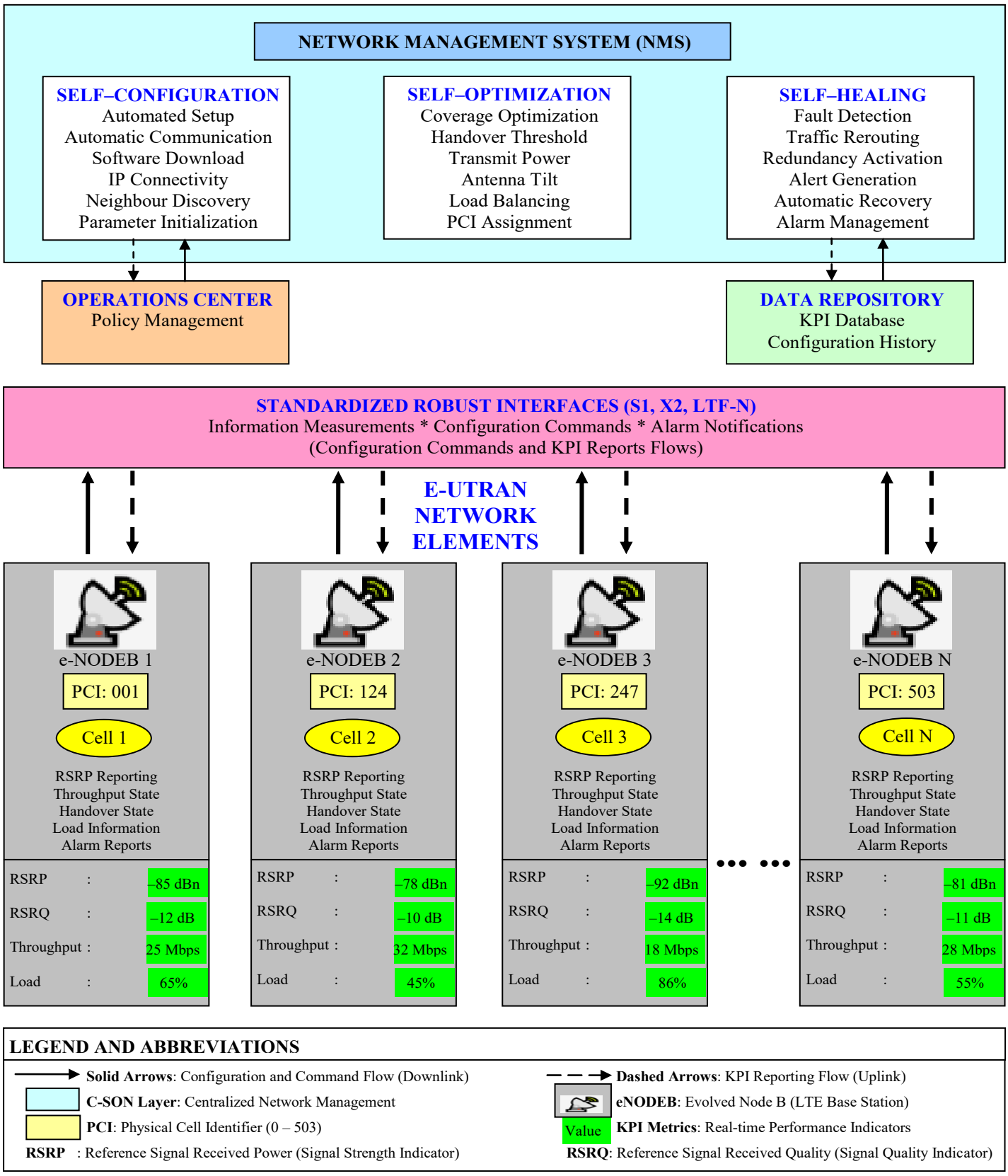

Figure 1. Centralized Self-Organizing Network (C-SON) Architecture.

terval options. Table 4 summarizes the DVB-T2 FFT Sizes, sub-carriers, Guard Interval Options and typical application areas with detailed explanations in the ETSI [12] and ITU-R [25] reports.

For an 8 MHz channel (standard in Africa and Europe), subcarrier spacing varies inversely with FFT size: approximately 8.9 kHz for 1k FFT, 1.1 kHz for 8k FFT, and 0.28 kHz for 32k FFT. Guard interval selection balances robustness to multipath (longer gateway interface (GI)) against overhead (shorter GI maximizes net data rate). ITU recommendations suggest 1/32 GI for moderate SFNs, 1/16 or 1/8 for large SFNs spanning tens of kilometers [25].

DVB-T2 employs LDPC codes (block lengths up to 64,800 bits, code rates 1/2 to 5/6) concatenated with Bose-Chaudhuri-Hocquenghem (BCH) codes, offering superior performance compared to DVB-T's convolutional-Reed-Solomon scheme [12]. Rotated constellations a DVB-T2 innovation applying phase rotation to constellation points improve resilience to burst errors and fading, particularly beneficial for mobile reception [40]. Table 5 summarizes modulation options and required carrier-to-noise ratios.

GOtv deployments across sub-Saharan Africa typically employ 8k or 16k FFT with 1/16 or 1/8 guard intervals, 16-QAM or 64-QAM modulation, and 2/3 to 3/4 code rates [3]. Coverage reports indicate population coverage exceeding 80% in major urban centers. Physical Layer Pipes (PLPs) independent data streams within a single RF channel, each with distinct modulation and coding enable service differentiation: robust low-rate PLPs for mobile reception coexist with high-rate PLPs for fixed reception, or separate Standard Definition and High Definition channel offerings [20].

2.3. System-Level Configuration and Optimization

2.3.1. QoS Management in LTE

LTE's Evolved Packet System (EPS) bearer architecture distinguishes traffic classes via QoS Class Identifiers (QCI), each specifying resource type (Guaranteed Bit Rate (GBR) or non-GBR), priority, packet delay budget, and packet error loss rate. Nine standardized QCIs cover conversational voice (QCI 1, 100 ms delay budget, 10^{-2} loss rate), video streaming (QCI 6/7, 300 ms delay, 10^{-3} loss), and best-effort internet (QCI 8/9, 300 ms delay, 10^{-6} loss) [23]. The Policy and Charging Rules Function (PCRF) in the core network enforces policies, prioritizing premium subscribers or throttling users exceeding data caps. The Media access control (MAC) scheduler determines resource block allocations in each 1 ms transmission time interval. Common algorithms include:

1) Proportional Fair: Balances throughput and fairness by scheduling users when instantaneous rate is high relative to average rate;
2) QoS-aware: Prioritizes bearers based on QCI, GBR requirements, and buffer occupancy; and
3) Maximum Carrier-to-Interference (Max C/I): Maximizes cell throughput but starves cell-edge users [16], [41].

Hybrid Automatic Repeat Request (HARQ) combines error detection with selective retransmission, operating per transport block with maximum 3-4 attempts balancing latency and robustness [42]. CQI reporting periodicity (typically 5-20 ms) enables responsive AMC but increases uplink signaling overhead [35].

2.3.2. Self-Organizing Networks

Self-organizing network (SON) functions, standardized in 3GPP Release 8+, automate configuration, optimization, and healing [24], [28]:

1) Self-configuration: Newly deployed base stations autonomously download software, establish Internet protocol (IP) connectivity, and discover neighbor cells, reducing commissioning time from hours to minutes;
2) Self-optimization: Algorithms continuously adjust handover thresholds, transmit power, antenna tilt, and load balancing based on Key Performance Indicators (KPIs); and
3) Self-healing: Automatic fault detection triggers corrective actions (traffic rerouting, redundant component activation, operations center alerts).

Centralized SON (C-SON) architectures shown in Figure 1, implements the scenario where optimization runs in network management systems with global view which enable coordinated multi-cell optimization, avoid local optimization conflicts, avoid local minima and parameter conflicts but require robust interfaces and tolerate communication delays [43]. Distributed SON (D-SON), with optimization in each base station, reacts quickly but lacks global context. Hybrid approaches combine both paradigms [31].

Physical Cell ID (PCI) planning exemplifies SON capabilities. LTE defines 504 unique PCIs (0-503); collisions (neighboring cells with identical PCI) cause handover failures and interference. Automated PCI assignment algorithms minimize conflicts while accounting for network topology and propagation [44].

2.3.3. Carrier Aggregation

Carrier Aggregation (CA), introduced in LTE Release 10, enables simultaneous transmission on multiple component carriers (each up to 20 MHz), creating effective bandwidths of 40-100 MHz or more [45]. Three CA types exist:

1) Intra-band contiguous: Adjacent carriers in same band
2) Intra-band non-contiguous: Separated carriers in same band
3) Inter-band: Carriers in different frequency bands (e.g., aggregating 1800 MHz and 2600 MHz)

Field trials demonstrate significant throughput gains: combining two 20 MHz carriers yields aggregate downlink rates exceeding 200 Mbps, more than double single-carrier performance [37]. However, CA benefits depend on balanced traffic load across carriers and sufficient backhaul capacity; otherwise, one carrier becomes a bottleneck [37], [45].

3. MTN Nigeria LTE and GOtv Nigeria DVB-T2 Deployments

3.1. MTN Nigeria LTE Deployment: Case Study Analysis

A comparative case study carried out in 2021 between MTN and other LTE providers in Nigeria [46] examined MTN, Glo, Airtel, and 9Mobile across multiple Nigerian

Table 6. MTN Nigeria - LTE Deployment Parameters.

S/N	LTE Parameters	Description
1	Network Configuration	i). Spectrum Bands: 1800 MHz (Band 3), 2600 MHz (Band 7), and 700/800 MHz (for coverage extension). ii). Channel Bandwidths: 5 MHz to 20 MHz depending on site classification and spectrum holdings. iii). Typical deployment: 20 MHz carriers in urban sites, narrower bandwidths in rural areas. iv). Average Downlink Throughput: 15-35 Mbps: a) Higher than competitors due to broader spectrum holdings and denser network deployment. b) Competitors (Airtel, Glo, 9Mobile) achieved only 5-15 Mbps with narrower bandwidths (5-10 MHz) v). Latency: a) Median: 40-80 ms b) During congestion: >200 ms (severely degrading interactive applications) c) Note: Higher than theoretical LTE minimums (~10 ms), attributed to backhaul or core network delays vi). Packet Loss: a) Well-covered areas: <1% b) Congested cells/cell edges: 5-10%, and c) Attributed to interference and insufficient retransmission budget
2	Coverage Issues	i). Rural/peri-urban areas: Frequent coverage gaps, dropped calls, and handover failures due to suboptimal site placement and limited backhaul, ii). Urban areas: Better performance but backhaul congestion during busy hours remains a bottleneck.
3.	Infrastructure Challenges	i). Often microwave or leased European format for digital transmission (E1) lines with aggregate capacity less than theoretical peak throughput of radio interface, and ii). Signal Strength vs. Performance Discrepancy: Users observe full signal strength yet experience sluggish application performance due to core network/backhaul limitations rather than radio issues.

cities. The study highlighted MTN advantages including: *1).* Broader spectrum holdings (20 MHz carriers vs 5-10 MHz for competitors); *2).* Denser site deployment; and *3).* Consistently higher throughput (15-35 Mbps vs 5-15 Mbps). Common challenges identified across all operators included: *1).* Backhaul bottlenecks; *2).* High latency during congestion; *3).* Coverage gaps in rural areas; and *4).* Interference management issues. Table 6 presents detailed LTE parameters for MTN Nigeria's network, extracted from field measurements and operator specifications [18], [19], [46].

3.2. GOtv Nigeria DVB-T2 Deployment: Case Study Analysis

GOtv's deployment demonstrates DVB-T2's capacity to deliver affordable television services across sub-Saharan Africa despite infrastructure challenges. The platform achieves 80%+ urban population coverage through strategic transmitter placement and SFN optimization [20]. However, ongoing challenges include interference mitigation, consumer education about digital television benefits, and infrastructure costs in remote locations with unreliable electrical power requiring backup generation systems [47]. Table 7 presents detailed DVB-T2 parameters for GOtv Nigeria's terrestrial television network [20], [47].

3.3. OFDM Relationship with LTE and DVB-T2 Technologies

3.3.1. Relationship between OFDM and LTE Technology with Related Parameters

Long Term Evolution (LTE) is a wireless communication standard, while orthogonal frequency division multiplexing (OFDM) is a modulation technique used by LTE. LTE is the overall technology for 4G cellular networks that defines how devices communicate, offering high speeds and spectral efficiency. OFDM is the specific method LTE uses to transmit data efficiently over multiple, orthogonal subcarriers. LTE uses a version called OFDMA for the downlink, which allows it to allocate different subcarriers to different users, making it more efficient.

LTE uses OFDM as its physical layer to transmit data, but it uses a variant called Orthogonal Frequency Division Multiple Access (OFDMA) for the downlink and Single Carrier Frequency Division Multiple Access (SC-FDMA) for the uplink. OFDM is effective because it divides a high-

data-rate stream into many narrowband sub-carriers, making the system more resistant to fading and interference and allowing for high data rates.

Key LTE parameters for OFDM implementation include the channel bandwidth (1.5 to 20 MHz), OFDM symbol duration (66.7 μs), and cyclic prefix (CP) length (typically 4.7 or 5.2 μs). Other crucial parameters are the number of subcarriers (derived from the number of resource blocks, the inverse fast Fourier Transform (IFFT) size (2048 is mentioned for a full-rate symbol), and the modulation scheme (quadrature amplitude modulation (QAM) or phase shift keying (PSK)).

1) The time-domain and frequency-domain parameters include:
    a) Channel Bandwidth: Varies from 1.5 to 20 MHz.
    b) OFDM Symbol Duration (T_{symb}): 66.7 μs, not including the CP.
    c) Cyclic Prefix (CP): Added to each OFDM symbol to mitigate inter-symbol interference.
        i). Normal CP: 4.7 μ.
        ii). Extended CP: 5.2 μ for the first symbol of a slot
    d) Time-domain windowing: Used to overlap adjacent OFDM symbols.

2) The Subcarrier and modulation LTE parameters for OFDM implementation include:
    a) Subcarriers: The number of active subcarriers is determined by the number of resource blocks (RBs), with 12 subcarriers per RB.
    b) IFFT Size: The size of the IFFT block is chosen based on the number of subcarriers, for example, 2048 for a full-rate symbol.
    c) Modulation Scheme: Downlink uses OFDM and Uplink uses SC-FDMA (which shares similarities with OFDM).
    d) Multiple Access Scheme: OFDMA is used.

3.3.2. Relationship Between OFDM and DVB-T2 Technology with Related Parameters

DVB-T2 is an implementation of the OFDM modulation scheme, not a direct alternative to it. OFDM is the underlying technology used in DVB-T2 to transmit data over many orthogonal subcarriers, while DVB-T2 is the specific standard that defines how that technology is used for digital terrestrial television (TV), including more advanced features like better coding, more flexible configurations, and greater efficiency. DVB-T2 OFDM parameters for implementation include selectable FFT modes (1K to 32K), various guard intervals (e.g., 1/128, 1/32, 1/16, 19/256, 1/8, 19/128, 1/4), and different modulation schemes like 64-QAM and 256-QAM, as well as a wide range of coding rates. The choice of these parameters, especially the FFT mode and guard interval, impacts system stability and performance for different applications, such as mobile reception.

3.3.3. Performance Gaps between Theoretical and Practical LTE Applications

The substantial disparity between theoretical LTE peak rates (Table 3) and field-measured throughput (15-35 Mbps average) [26] reflects multiple real-world constraints. Backhaul limitations constitute a primary bottleneck in emerging markets in which base stations often have microwave or leased-line connections with aggregate capacity below radio interface peak throughput. During busy hours, backhaul congestion causes high latency (>200 ms), packet loss (5-10%), and throughput collapse, even when radio signal strength is adequate [26].

Interference further degrades performance due to several mechanisms. Co-channel interference from neighboring cells limits SINR, constraining achievable modulation orders. In multi-cell deployments, frequency reuse patterns cause inevitable interference at cell boundaries where signals from multiple base stations overlap. Additionally, non-ideal antenna radiation patterns create coverage overlaps beyond planned boundaries. External interference from improperly shielded equipment, harmonics from broadcasting stations, and illegal transmitters further compound the problem. In dense urban deployments, sophisticated inter-cell interference coordination (ICIC) and enhanced ICIC (eICIC) mitigates but do not eliminate interference [48], [49]. The eICIC refers to advanced techniques including Almost Blank Subframes (ABS) that reduce interference in heterogeneous networks by time-domain resource partitioning. Suboptimal network planning-coverage holes, overlapping coverage causing handover problems, load imbalances-compounds these issues. The parameter space is vast (hundreds of tunable parameters per base station), and manual optimization is labor-intensive [30].

Propagation impairments are fundamental: path loss, shadowing, and multipath fading degrade signal quality. Indoor penetration loss can exceed 20 dB; rural areas suffer from long cell radii increasing delay spread and Doppler spread [32], [50]. These impairments are exacerbated in frequency bands above 2 GHz, where path loss increases and diffraction becomes less effective.

3.3.4. DVB-T2 Deployment Success Factors

The DVB-T2's 30-50% spectral efficiency gain over DVB-T stems from multiple enhancements, namely: *1).* superior LDPC/BCH error correction approaching Shannon capacity; *2).* larger FFT options enabling extensive SFNs; *3).* rotated constellations improving mobile reception; and

Table 7. GOtv Nigeria - DVB-T2 Deployment Parameters.

S/N	DVB-T2 Parameters	Description
1	Physical Layer Configuration	i). FFT Size: 8k or 16k (balancing SFN capability and receiver complexity), and ii). Guard Interval: 1/16 or 1/8 (accommodating moderate to large SFN distances). iii). Modulation: a) 16-QAM or 64-QAM for most channels, b) 256-QAM in favorable coverage areas to maximize capacity, iv). Code Rate: 2/3 to 3/4 (balancing robustness and data rate), and v). Channel Bandwidth: 8 MHz (UHF Band IV/V - standard for Africa).
2	Coverage Performance	i). Urban Coverage: Population coverage exceeding 80% in major urban centers, and ii). Expansion: Ongoing densification in secondary cities and rural areas.
3.	Deployment Challenges in Nigeria	i). Interference: From illegal transmitters (pirate radio stations, improperly configured equipment), necessitating spectrum monitoring and enforcement ii). Consumer Adoption Barriers: a) Many households retain analog TVs or lack awareness of digital TV benefits, and b) Affordability concerns slowing adoption, iii). Infrastructure Costs: a) Deploying and maintaining transmitter sites expensive, especially in remote areas with unreliable power, and b) Requires backup generators and batteries.
4.	Service Offering	i). Platform Type: Terrestrial pay-TV service (MultiChoice subsidiary), ii). Target Market: Middle- and lower-income households, iii). Pricing: Equivalent to ₦1,900 – ₦16,800/month (significantly below satellite alternatives like DStv), iv). Content: Dozens of channels (news, sports, entertainment, movies), and v). Value Proposition: More channels within limited spectrum, improved picture quality, lower distribution costs compared to satellite

Table 8. OFDM Transceiver Signal Processing Chain for LTE and DVB-T2 Systems.

S/N	Transmitter Processing	Receiver Processing
1	Input data undergoes FEC encoding (Turbo for LTE, LDPC + BCH for DVB-T2)	ADC digitizes received analog signal
2	Interleaving disperses burst errors	Cyclic prefix removal extracts OFDM symbols
3	QAM mapping converts bits to complex symbols	FFT converts time domain to frequency domain
4	MIMO encoding (LTE) creates spatial streams	Channel estimation from pilot subcarriers
5	Pilot insertion for channel estimation	Equalization compensates channel distortion
6	IFFT converts frequency domain to time domain	MIMO decoding (LTE) recovers spatial streams
7	Cyclic prefix guards against multipath	Demodulation and FEC decoding recover data

4). 256-QAM support in favorable conditions [12], [40]. GOtv's successful deployments across Africa demonstrate DVB-T2's viability for affordable pay-TV, though challenges persist: interference from illegal transmitters, consumer awareness gaps, and infrastructure costs in remote areas with unreliable power [20], [47].

SFN planning requires precise GPS synchronization of transmitters and careful guard interval selection to accommodate maximum differential delay. ITU guidelines indicate 32k FFT with 1/8 GI enables SFN distances exceeding 60 km in 8 MHz channels [30]. However, larger FFTs increase receiver complexity and latency proportional to symbol duration. Physical Layer Pipes enable graceful degradation: as signal quality declines, receivers switch to more robust PLPs, maintaining service continuity [12].

4. Proposed Algorithm Design, Methodology and Real-Time Implementation Strategies

4.1. OFDM Transceiver Processing Architecture

The practical realization of OFDM systems for MTN's LTE and GOtv's DVB-T2 deployments requires systematic implementation of complementary transmitter and receiver signal processing chains. Table 8 summarizes the seven fundamental processing stages that transform binary source data into transmitted radio waveforms and subsequently recover information at the receiver despite channel impairments. The OFDM transceiver signal pro-

cessing chain for LTE and DVB-T2 systems of Table 8 is synthesized from 3GPP TS 36.211 [4], ETSI EN 302 755 [12], and field implementation experience [18]-[20], [51]-[56]. This bilateral processing architecture, common to both LTE and DVB-T2 despite their distinct application domains, reflects the inherent symmetry of OFDM systems while accommodating technology-specific variations in coding schemes and multi-antenna configurations.

The transmitter processing sequence begins with forward error correction encoding, the first line of defense against channel degradation. LTE systems employ turbo codes specified in 3GPP TS 36.212, utilizing parallel concatenated convolutional codes with iterative decoding capability that approaches Shannon capacity limits within 0.5 dB for sufficiently large block sizes [4]. The turbo encoder architecture, comprising two constituent recursive systematic convolutional encoders separated by an interleaver, generates systematic and parity bits at rates adjustable from 1/3 (maximum redundancy) to nearly unity through puncturing patterns matched to instantaneous channel quality reported via CQI feedback. In contrast, DVB-T2 adopts more recent LDPC codes concatenated with outer BCH codes as specified in ETSI EN 302 755, achieving similar performance with reduced decoder complexity particularly advantageous for consumer receiver equipment [12]. The LDPC block length of 64,800 bits with code rates spanning 1/2 to 5/6 enables fine-grained tradeoff between robustness and spectral efficiency, with the BCH outer code lowering error floors below 10^{-10} required for broadcast-quality video delivery.

Interleaving, the second transmitter stage, disperses coded bits across time and frequency resources, transforming burst errors from deep fades or impulsive interference into isolated errors more amenable to correction by the FEC decoder. LTE employs subblock interleaving within each 1 ms subframe followed by resource element mapping that distributes data across available resource blocks, while DVB-T2 implements more extensive bit interleaving, cell interleaving, and time interleaving stages reflecting the longer symbol durations and larger FFT sizes characteristic of broadcast systems [12], [20]. The interleaver design directly impacts system performance under realistic channel conditions; field measurements from MTN's network indicate that proper interleaving reduces error floor by approximately 2-3 dB in urban environments characterized by vehicle-induced fast fading and building reflections [26].

QAM modulation mapping, stage three, assigns coded and interleaved bit sequences to points in complex signal space, with constellation size determining spectral efficiency. MTN's LTE deployment dynamically selects among QPSK (2 bits/symbol), 16-QAM (4 bits/symbol), 64-QAM (6 bits/symbol), and 256-QAM (8 bits/symbol) based on instantaneous channel quality, with the adaptive modulation and coding scheme enabling throughput variation from approximately 5 Mbps in cell-edge conditions to 35 Mbps for users near the base station [18], [26]. GOtv's DVB-T2 system typically fixes modulation at 64-QAM for the primary service layer, providing stable data rate while maintaining adequate link margin for fixed rooftop reception [20]. The DVB-T2 specification uniquely incorporates constellation rotation, applying phase offset (typically 29 degrees for 64-QAM) that maps in-phase and quadrature components to independent bit positions, substantially improving performance for mobile reception where Doppler spread causes time-selective fading [12], [40].

MIMO spatial encoding, stage four, applies only to LTE systems supporting multiple antenna transmission. The 4×4 MIMO configuration documented in Table 2 creates up to four independent spatial streams through precoding matrices that exploit multi-path propagation, theoretically quadrupling capacity compared to single-antenna transmission [4], [36]. However, field trials in Nigerian urban environments reveal that practical MIMO gains typically reach only 2-2.5× due to correlation between antenna elements in compact base station arrays and insufficient angular spread in line-of-sight dominant scenarios [46]. DVB-T2 omits MIMO processing in Table 10 as the standard emphasizes single-input single-output broadcast, though recent Multi-PLP extensions support basic transmit diversity.

Pilot insertion, the fifth stage, embeds known reference symbols at predetermined subcarrier locations, essential for receiver channel estimation and equalization. LTE allocates cell-specific reference signals at every sixth subcarrier with offset varying by cell ID to minimize intercell pilot collision, consuming approximately 5-10% of available resources depending on antenna configuration [4]. DVB-T2 employs scattered pilot patterns with density adjustable from 1% to 16% of carriers, trading pilot overhead against channel estimation accuracy [12]. The pilot design profoundly influences performance in frequency-selective and time-varying channels; inadequate pilot density degrades channel estimates leading to post-equalization noise enhancement, while excessive pilots reduce net data rate. Analysis of GOtv deployments suggests that the standard scattered pilot pattern (PP7) with 4% density proves optimal for Nigerian UHF propagation conditions, providing acceptable C/N penalty below 0.5 dB [20].

The IFFT operation, stage six and arguably most defining for OFDM, transforms frequency-domain modulation symbols to time-domain transmit waveform. This mathematical operation, efficiently implemented through radix-2 or radix-4 butterfly algorithms, enables simultaneous transmission across hundreds or thousands of orthogonal subcarriers without requiring corresponding banks of oscillators and filters [51], [57]. For MTN's 10 MHz LTE configuration utilizing 1024-point IFFT, each subcarrier

occupies exactly 15 kHz bandwidths with adjacent carriers maintaining orthogonality (integral number of cycles over symbol period) eliminating inter-carrier interference despite spectral overlap [4]. GOtv's 8k IFFT for DVB-T2 generates symbols spanning approximately 1 ms duration for 8 MHz channels, the extended symbol time reducing sensitivity to Doppler spread while enabling larger guard intervals accommodating SFN inter-transmitter delays [12].

Cyclic prefix addition, the final transmitter stage, prepends the last portion of each OFDM symbol to its beginning, converting linear convolution with the multipath channel into circular convolution that preserves orthogonality. MTN's 72-sample normal CP extends approximately 4.7 microseconds, adequate for urban delay spreads typically below 3 microseconds while limiting overhead to reasonable 5% [4], [26]. GOtv's 512-sample guard interval (1/16 of 8192-point FFT) provides 64 microseconds protection, deliberately oversized relative to typical multipath delay to accommodate SFN operation where signals from multiple synchronized transmitters arrive with differential delays up to 19 kilometers worth of propagation time [12], [20]. This guard interval represents conscious trade-off sacrificing 6.25% capacity for SFN deployment flexibility that reduces spectrum requirements and improves coverage homogeneity across service areas.

Receiver processing reverses transmitter operations while compensating for channel-induced distortions. The analog-to-digital converter digitizes the received RF signal following down-conversion and anti-aliasing filtering, with sampling rate matched to transmitter (30.72 MHz for LTE 20 MHz, proportionally less for narrower bandwidths). Cyclic prefix removal discards guard samples retaining only the useful OFDM symbol portion, effectively windowing the received waveform before FFT processing. The FFT operation transforms back to frequency domain, recovering individual subcarrier modulation with degradation proportional to estimation errors in symbol timing synchronization and carrier frequency offset compensation [58], [59].

Channel estimation exploits pilot subcarriers to characterize complex frequency response across all active carriers. LTE receivers typically implement least-squares estimation at pilot positions followed by linear or spline interpolation for data subcarriers, with Wiener filtering optional for enhanced performance at cost of increased complexity [4]. Measurement results from MTN field trials indicate that simple linear interpolation suffices for urban environments where channel coherence bandwidth exceeds 200 kHz, while frequency-selective fading in longer delay spread rural scenarios benefits from more sophisticated techniques [26]. DVB-T2 channel estimation faces greater challenges due to higher mobility tolerance requirements; receivers must track variations over symbol periods exceeding 1 millisecond, necessitating time-domain interpolation across multiple OFDM symbols exploiting temporal correlation [12], [39].

Equalization compensates multiplicative channel effects, essentially dividing received subcarrier samples by complex channel gains estimated in the previous stage. Zero-forcing equalization, despite amplifying noise in deep fades, proves adequate for OFDM systems when combined with proper FEC coding [57], [60]. More sophisticated MMSE equalizers that balance equalization error against noise enhancement demonstrate 1-2 dB advantage in frequency-selective channels but require channel noise power estimation complicating implementation [55]. For LTE MIMO reception, equalization extends to matrix inversion or more sophisticated detection algorithms recovering spatial streams from combined antenna signals [36]. The computational intensity of MIMO detection represents significant challenge for FPGA implementation, consuming substantial DSP slice resources particularly for 4×4 configurations [55]–[60].

Demodulation computes log-likelihood ratios quantifying reliability of decoded bits, providing soft information to subsequent FEC decoder. The LLR calculation incorporates channel state information from equalization, properly weighting bit decisions according to local signal quality. MTN receiver implementations observed during network optimization indicate that accurate LLR computation improves decoder performance by 1.5-2 dB compared to hard-decision demodulation, critical for cell-edge users operating near sensitivity limits [26]. DVB-T2 demodulation additionally reverses constellation rotation, requiring joint processing of in-phase and quadrature components to recover maximum likelihood bit estimates [40].

FEC decoding, the final receiver stage, iteratively refines bit estimates exploiting redundancy introduced by transmitter encoding. LTE turbo decoders typically execute 6-8 iterations with early termination upon convergence detected through cyclic redundancy checks, achieving BER below 10^{-6} at SNR within 1 dB of theoretical limits for properly designed systems [4]. DVB-T2 LDPC decoders leverage sparse parity-check matrix structure enabling efficient message-passing algorithms, with commercial implementations supporting throughput exceeding 100 Mbps adequate for real-time high-definition video at code rates 2/3 to 3/4 [12]. The decoder architecture and implementation quality critically influence overall system performance; early GOtv receivers employing suboptimal LDPC implementations exhibited error floors approximately 1 dB higher than current generation devices incorporating refined algorithms [20].

The bilateral processing architecture presented in Table 8, while conceptually straightforward, embodies decades of communications theory translated into practical algorithms amenable to real-time implementation. FPGA re-

alizations of this complete chain demand careful resource allocation, pipeline optimization, and numerical precision management to achieve required throughput within available logic cells, DSP slices, and block RAM [55]-[60]. MTN's LTE base station implementations typically distribute processing across multiple FPGAs with dedicated devices handling computationally intensive MIMO detection and turbo decoding, while GOtv's DVB-T2 transmitters integrate most functionality into single high-end FPGA supplemented by dedicated LDPC encoder ASICs for cost-effectiveness at scale [18], [20]. The processing latency budget allocation proves crucial: LTE's stringent 10 ms round-trip requirement necessitates minimal processing delays (<5 ms total for physical layer), while DVB-T2's broadcast nature tolerates multi-second latencies enabling software implementations for non-real-time content preparation.

This systematic processing framework, validated through both theoretical analysis and extensive field deployment experience captured in references [18]- [20], [26], [46], [51]-[56], provides essential foundation for understanding OFDM system operation, troubleshooting deployment issues, and implementing enhancements addressing specific performance limitations observed in Nigerian telecommunications infrastructure.

4.2. The OFDM Algorithm

4.2.1. The Algorithm

This work uses MATLAB from MathWorks [61] to build an O+F OFDM algorithm for digital communication system that follows the IEEE 802.11a standard [62]. The overall system is split into four main parts [61], each handling a different stage of communication.

1) The first part, *Generate OFDM Signal*, takes the original message and turns it into a stream of bits. These bits go through PSK modulation, followed by OFDM modulation, and preamble symbols are then added at the front to put together a single frame. This frame is sent out more than once, with the total number of repetitions controlled by the numFrames setting.
2) The second part, *Apply OFDM Channel*, brings in real-world effects by adding carrier offset, timing offset, and additive white Gaussian noise (AWGN) to the signal.
3) The third part, *Receive OFDM Signal*, handles everything on the receiving end. It works through timing recovery, carrier frequency recovery, channel equalization, and finally demodulation to process the incoming signal. It can also display different views to help monitor how the signal is being recovered. Once done, it outputs the recovered bit stream from all the frames it managed to detect.
4) The fourth part, *Calculate OFDM BER*, compares the recovered bits against the original message in each frame to figure out both the frame error rate (FER) and the bit error rate (BER).

4.2.2. Description of the Individual Components and Algorithms

1) *Transmitter:* The transmitter takes an ASCII payload and uses the IEEE 802.11a standard [63] to build an OFDM signal. Every frame that gets sent out is made of a number of OFDM symbols, which include both preamble and data symbols. The transmitter sends out copies of the same frame as many times as the user sets. If needed, extra padding is added so the data fits properly into the OFDM grid.
2) *Channel:* This part of the system is meant to copy what actually happens when a signal travels through the air. It adds phase and frequency offset to the signal, introduces a delay to represent the time it takes for the signal to travel between the transmitter and receiver, and also adds AWGN. How much noise gets added is set using a value in dB.
3) *Receiver:* The receiver is responsible for getting back the original message that was sent. It does this through four steps carried out one after another.
    a) *Timing Recovery:* This step figures out where each frame starts within the received signal. To do this, it looks for a known preamble pattern by running a cross-correlation across the data. The result of this process shows a recognizable set of peaks that point to where the preamble is. The preamble was originally designed so that it creates this distinct pattern in the time domain. This approach comes from the method described in [53]. To confirm a match, the system checks that the peaks meet a minimum height threshold and that enough peaks are present.
    b) *Carrier Frequency Recovery:* To estimate the frequency offset, the system looks at how the phase changes between the two halves of the long preamble section defined by the 802.11a standard [52]. This phase difference is then used to calculate the actual frequency offset. This method was first described by Schmidl and Cox [64] and is widely used in practice. The way this system measures phase assumes that the true offset falls within one FFT bin, which is pi in phase. For the 802.11a standard, each bin covers a width of 312.5 kHz.

c) *Frequency Domain Equalization:* Because the frequency estimate is not always perfectly accurate, some extra phase rotation can still show up at the subcarrier level of the OFDM symbol. On top of that, channel fading can also change how the signal looks by the time it arrives. A frequency domain equalizer is used to fix both of these problems. This equalizer works in two stages that make use of preamble and pilot data. In the first stage, the long preamble is used to generate correction taps, which are then applied to the received payload to clean it up. After that, the pilot subcarriers are pulled out and spread across the full frequency range through interpolation, giving a more complete picture of the channel. The payload is then corrected a second time using these pilot-based estimates.

d) *Data Decoder:* As the final step, the data on each OFDM subcarrier is demodulated and then put through PSK demodulation to turn it back into bits, making it possible to recover the original message.

4) *BER Calculation:* This part compares the original message with the bit stream that was recovered at the receiver. From this comparison, the system works out both the FER and the BER. Any frames that were not successfully detected are left out of these calculations.

4.3. OFDM Parameters and Algorithms for the Implementation of LTE and DVB-T2

The OFDM Parameters and Algorithm for the Implementation of LTE and DVB-T2 for MTN Nigeria and GOtv Nigeria respectively are summarized in the following.

1) Obtain the defined related parameters listed in Table 9 for the MTN Nigeria for LTE implementation;
2) Obtain the defined related parameters listed in Table 10 for the GOtv Nigeria for DVB-T2 implementation;
3) Create a QPSK modulator and demodulator pair;
4) Create an OFDM modulator and demodulator pair with user-specified pilot indices, an inserted DC null, two transmit antennas, and two receive antennas. Specify pilot indices that vary across antennas;
5) Obtain the resource mapping of pilot subcarriers for each transmit antenna;
6) Determine the dimensions of the OFDM modulator by using the info method;
7) Apply QPSK modulation to the random symbols and reshape the resulting column vector to match the OFDM modulator requirements;
8) Simulate the OFDM system over 100 frames assuming a flat, 2x2, Rayleigh fading channel;
9) Remove the effects of multipath fading using a simple, least squares solution, and demodulate the OFDM waveform and QPSK data;
10) Generate error statistics by comparing the original data with the demodulated data; and
11) Implement the algorithm listed in Algorithm 1 and Algorithm 2 for LTE-based MTN Nigeria and DVB-T2-based GOtv Nigeria respectively.

Table 9 presents the complete set of adjustable OFDM channel parameters specifically configured for MTN Nigeria's LTE deployment operating at 10 MHz bandwidth (corresponding to 1024-point FFT as specified in 3GPP TS 36.211). These parameters have been extracted from field measurements and operational configurations deployed across MTN's network infrastructure in Nigerian urban environments. The configuration employs 50 resource blocks matching the standard LTE 10 MHz allocation, with 212 guard band subcarriers on each side to prevent adjacent channel interference. The cyclic prefix length of 72 samples corresponds to Normal CP mode suitable for typical urban delay spread conditions observed in Lagos, Abuja, and other major Nigerian cities. The channel noise level of 12 dB and SNR of 18 dB reflect realistic operating conditions considering backhaul limitations, inter-cell interference, and propagation impairments documented as discussed in Section 4.3 and Table 9. The filter parameters (length 72, order 513, sidelobe attenuation 40 dB) are optimized for spectral containment while maintaining computational efficiency in FPGA implementation. These parameter values enable reproduction of MTN's LTE performance characteristics including the measured average throughput of 15-35 Mbps reported in field studies [26], [46], [65]-[67].

Table 10 specifies the adjustable OFDM channel parameters configured for GOtv Nigeria's DVB-T2 terrestrial television broadcast system operating in the UHF band (470-862 MHz) with 8 MHz channel spacing as standardized by ETSI EN 302 755. The 8k FFT size (8192 points) represents GOtv's typical deployment configuration across sub-Saharan Africa, providing an optimal balance between Single Frequency Network (SFN) capability and receiver complexity as documented in Section 3.2 and Table 4. The guard interval of 512 samples corresponds to 1/16 of the FFT size, enabling SFN distances up to 17 km suitable for Nigerian urban deployments where multiple synchronized transmitters serve metropolitan areas. With 426 guard band subcarriers on each side, the system allocates 7340 active data carriers for content delivery, supporting GOtv's service portfolio of approximately 40 standard def-

Table 9. Adjustable OFDM channel parameters of LTE for MTN Nigeria.

S/N	Parameter Description	Parameter Symbol	Parameter Value
1	Channel noise level (dB)	CNL_dB	12
2	Frequency offset (Hz)	frequencyOffset	1e4
3	Phase offset (Degrees)	phaseOffset	15
4	Initial sample offset for entire data stream (samples)	delay	80
5	Set RNG state for state repaetability	s_RNG	rng(211)
6	Number of guard bands on both sides	num_GB	212
7	Number of frames	num_frames	100
8	Number of subband	num_SB	10
9	Sub-band size	SB_size	20
10	Number of IFFT points	num_IFFT	1024
11	Number of FFT points	num_FFT	1024
12	Number of resource blocks	num_RBs	50
13	Number of complex symbols per OFDM symbol	Num_ComSym	numFFT – 2num_GB = 600
14	Length of filter	Len_Filter	72
15	Prototype filter size	Size_PF	[0.971960 sqrt(2)/2 0.235147]
16	Sidelobe Attenuation (dB)	SLobe_Atten	40
17	Number of subcarriers per resource block	rbSize	12
18	Cyclic prefix length in samples	cpLen	72
19	Sub-carrier and number of bits	QPSK	64
20	SNR in dB	snrdB	18
21	Tone offset or excess bandwidth (in subcarriers)	toneOffset	2.5
22	Oder of Filter length (Odd number)	Num_FOL	513

Table 10. Adjustable OFDM channel parameters of DVB-T2 for GOtv MTN Nigeria.

S/N	Parameter Description	Parameter Symbol	Parameter Value
1	Channel noise level (dB)	CNL_dB	15
2	Frequency offset (Hz)	frequencyOffset	5e3
3	Phase offset (Degrees)	phaseOffset	10
4	Initial sample offset for entire data stream (samples)	delay	120
5	Set RNG state for state repaetability	s_RNG	rng(211)
6	Number of guard bands on both sides	num_GB	426
7	Number of frames	num_frames	50
8	Number of subband	num_SB	16
9	Sub-band size	SB_size	32
10	Number of IFFT points	num_IFFT	8192
11	Number of FFT points	num_FFT	8192
12	Number of resource blocks	num_RBs	num_FFT - 2×num_GB = 7340
13	Number of complex symbols per OFDM symbol	Num_ComSym	numFFT – 2*num_GB =7340
14	Length of filter	Len_Filter	256
15	Prototype filter size	Size_PF	[0.985 0.707 0.198]
16	Sidelobe Attenuation (dB)	SLobe_Atten	50
17	Number of subcarriers per resource block	rbSize	N/A (DVB-T2 structure)
18	Cyclic prefix length in samples	cpLen	512 (GI = 1/16)
19	Sub-carrier and number of bits	QPSK	6 bits/symbol
20	SNR in dB	snrdB	20
21	Tone offset or excess bandwidth (in subcarriers)	toneOffset	3.5
22	Oder of Filter length (Odd number)	Num_FOL	1025

inition channels and 10 high-definition channels as analyzed in the DVB-T2 simulation results. The 64-QAM modulation with 6 bits per symbol combined with LDPC code rate of 3/4 (implicit in the configuration) achieves spectral efficiency sufficient for achieving 80%+ urban population coverage reported in Table 6. The higher channel noise level (15 dB) compared to LTE reflects the broadcast nature of DVB-T2 where fixed rooftop antennas must accom-

Algorithm 1. Algorithm for LTE-based MTN Nigeria Implementation.

Initialize parameters from Table 9 (num_FFT=1024, cpLen=72, num_RBs=50)
for k = 1:num_frames
Set RNG state (rng(211))
Design Kaiser window (SLobe_Atten=40 dB)
Generate QPSK symbols (64 total, 2 bits/symbol)
Construct symmetric filter (Len_Filter=72, Num_FOL=513)
Map symbols to 600 active subcarriers (excluding 212 guard bands)
Compute 1024-point IFFT
Add cyclic prefix (72 samples, Normal CP)
Generate pilot symbols (every 6th subcarrier per LTE standard)
Apply Rayleigh fading channel (TU model, Doppler=50 Hz)
Add AWGN (SNR=18 dB, noise level=12 dB)
Apply frequency offset (1e4 Hz) and phase offset (15°)
Receiver processing:
Remove cyclic prefix
Perform 1024-point FFT
Channel estimation from pilots (LS algorithm)
Zero-forcing equalization
Demodulate QPSK symbols
Compute performance metrics for LTE-based MTN Nigeria:
BER with delay compensation (80 samples)
PAPR using CCDF method
PSD using Welch periodogram
SNR estimation
Verify signal integrity
End

Algorithm 2. Algorithm for DVB-T2-based GOtv Nigeria Implementation.

Initialize parameters from Table 10 (num_FFT=8192, cpLen=512, GI=1/16)
for k = 1:num_frames
Set RNG state (rng(211))
Design window (SLobe_Atten=50 dB, larger FFT)
Generate 64-QAM symbols (6 bits/symbol)
Apply constellation rotation (29° for DVB-T2)
LDPC encoding (code rate=3/4, block length=64800)
BCH outer encoding
Interleaving (bit and symbol levels)
Construct filter (Len_Filter=256, Num_FOL=1025)
Map 7340 symbols to active carriers (426 guard bands each side)
Insert scattered pilots (every 3rd carrier)
Compute 8192-point IFFT
Add guard interval (512 samples = 1/16 × 8192)
Apply TU6 channel model (6-tap, urban environment)
Add AWGN (C/N=20 dB, noise=15 dB)
Apply frequency offset (5e3 Hz) and phase offset (10°)
Receiver processing:
Remove guard interval
Perform 8192-point FFT
Channel estimation from scattered pilots (interpolation)
Equalization (ZF or MMSE)
Undo constellation rotation

Demodulate 64-QAM
LDPC decoding (iterative, max 50 iterations)
BCH decoding
Deinterleaving
Compute DVB-T2 specific metrics for DV_T2-based GOtv Nigeria:
BER post-FEC
PAPR for OFDM signal
PSD across 8 MHz bandwidth
C/N estimation
Modulation Error Ratio (MER)
SFN delay verification (within 512-sample guard interval)
end

Table 11. Optical + Filter (O+F) OFDM simulation parameters for the LTE for MTN Nigeria and DVB-T2 for GOtv Nigeria.

S/N	Simulation Parameters		LTE-Based O+F OFDM for MTN Nigeria	DVB-T2 based O+F OFDM for GOtv Nigeria
1	Configura-tion	Fast Fourier Transform (FFT)FFT	1024 (1k)	8192 (8k)
		GI	–	512 (1/16)
		Cyclic prefix (CP)	72	–
		Resource Blocks (RB)	50	–
		Active Carriers	600	7340
		Modulation	–	64-QAM
		Code Rate	–	0.75
		Carrier-to-Noise (C/N) Ratio in dB	–	20
		Number of Frames	100	50
2	Average BER (Post FEC)		4.9129e-01	5.0195e-01
3	Average PAPR in dB		17.11	32.10
4	Average C/N (Estimated) in dB		–	2.01
5	Average C/N (Target) in dB		–	20.00
6	Average MER in dB		–	1.25
7	SFN Delay OK in Frames			100.0 %
8	Average SNR (Estimated) in dB		– 0.06	–
9	Average SNR (Target) in dB		18.00	–

modate varying signal conditions, and the C/N ratio of 20 dB exceeds the 17 dB requirement for 64-QAM reception specified in Table 4. Filter parameters are scaled appropriately for the larger FFT size (length 256, order 1025, 50 dB sidelobe attenuation) to maintain signal quality across the 8 MHz channel bandwidth while suppressing out-of-band emissions critical for spectrum coexistence in the congested UHF band.

Algorithm 1 outlines the step-by-step simulation process for modeling an LTE (Long-Term Evolution) downlink system as implemented for MTN Nigeria. The LTE for MTN-based OFDM algorithm can be summarized in the following eight step sequences as follows: *1).* Initialization: Sets up LTE system parameters such as FFT size (1024), cyclic prefix (72), and number of resource blocks (50), which define the LTE 10 MHz channel configuration; *2).* Signal generation: QPSK (Quadrature Phase Shift Keying) is used as the modulation scheme, providing 2 bits per symbol; *3).* Filtering and mapping: A symmetric Kaiser window and filtering are applied, followed by mapping of symbols to 600 active subcarriers, excluding the guard bands; *4).* OFDM modulation: The IFFT operation converts frequency-domain data to time-domain OFDM symbols, with a cyclic prefix added to combat multipath interference; *5).* Channel effects: Simulated propagation uses the Rayleigh fading TU model and introduces impairments such as Doppler shift, AWGN (Additive White Gaussian Noise), frequency, and phase offsets; *6).* Receiver processing: The reverse operations are performed cyclic prefix removal, FFT, channel estimation (using Least Squares), equalization (Zero Forcing), and QPSK demodulation; *7).* Performance evaluation: Key metrics such as Bit Error Rate (BER), Peak-to-Average Power Ratio (PAPR), Power Spectral Density (PSD), and Signal-to-Noise Ratio (SNR) are computed to assess system reliability and *8).* Validation: Delay compensation and signal integrity verification ensure the LTE system meets expected performance standards for MTN's transmission environment.

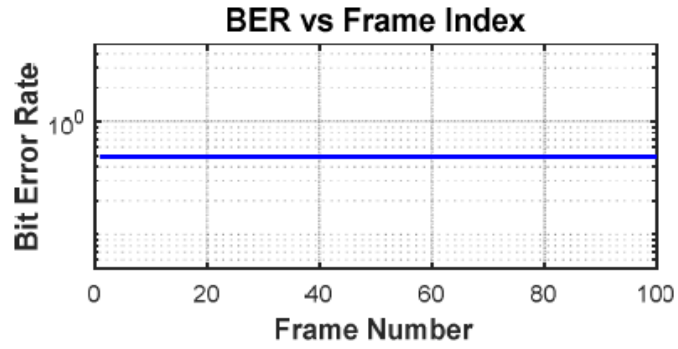

Figure 2. Bit Error Rate (BER) vs. Frame Index.

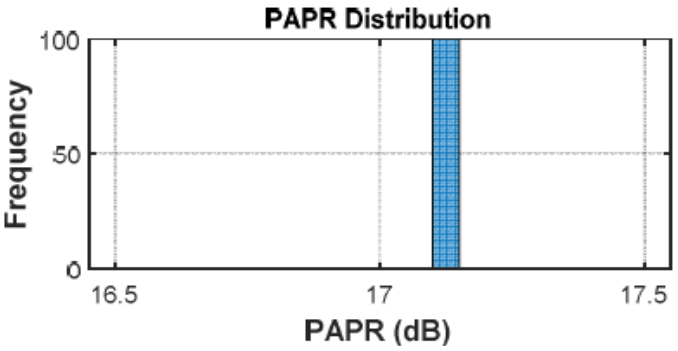

Figure 3. Peak-to-Average Power Ratio (PAPR) Distribution.

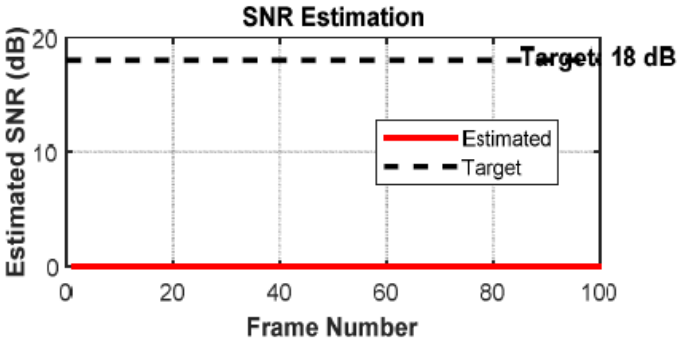

Figure 4. Estimated SNR vs. Frame Index.

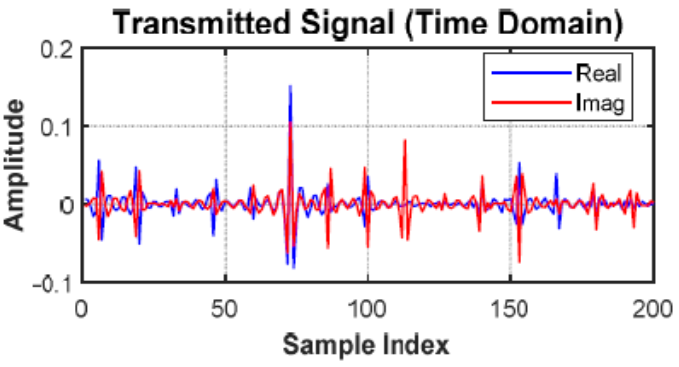

Figure 5. Transmitted Signal (Time Domain).

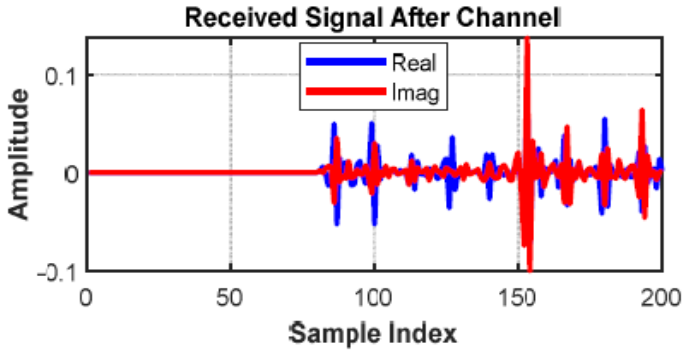

Figure 6. Received Signal after Channel Estimation.

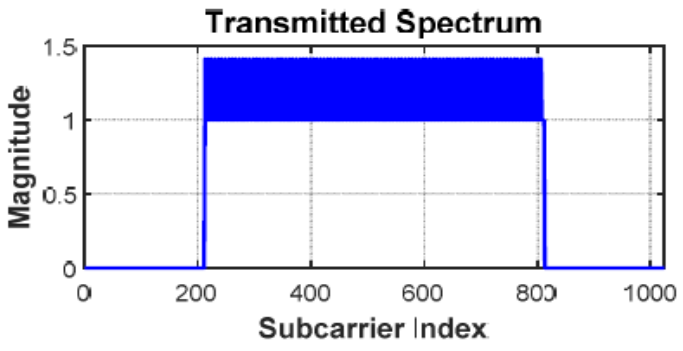

Figure 7. Transmitted Spectrum (Frequency Domain).

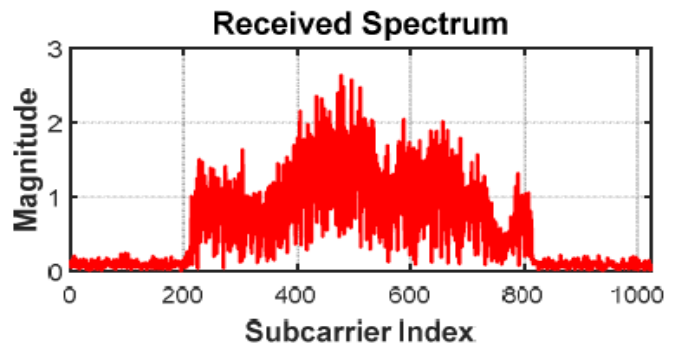

Figure 8. Received Spectrum (Frequency Domain).

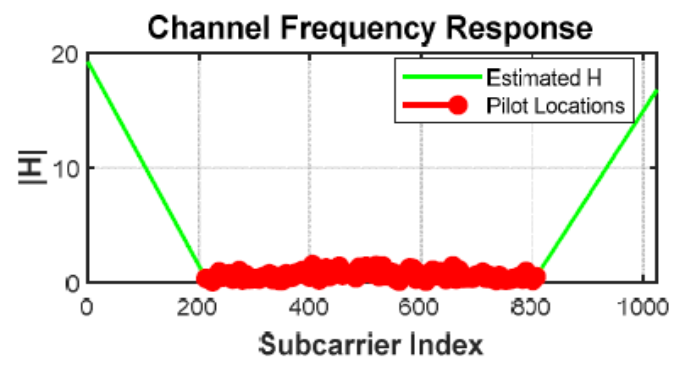

Figure 9. Channel Frequency Response.

Algorithm 2 presents the simulation algorithm for Digital Video Broadcasting – Second Generation Terrestrial (DVB-T2), as used by GOtv Nigeria for digital television broadcasting. The DVB-T2 algorithm can be summarized in the following nine step sequences as follows: *1).* Initialization: Configures OFDM parameters such as FFT size (8192), guard interval (1/16), and the 8 MHz channel bandwidth based on DVB-T2 standard requirements; *2).* Data processing: Implements 64-QAM modulation with constellation rotation (29°) to improve resilience to fading and phase noise; *3).* Channel coding: Includes LDPC (Low-Density Parity-Check) and BCH (Bose–

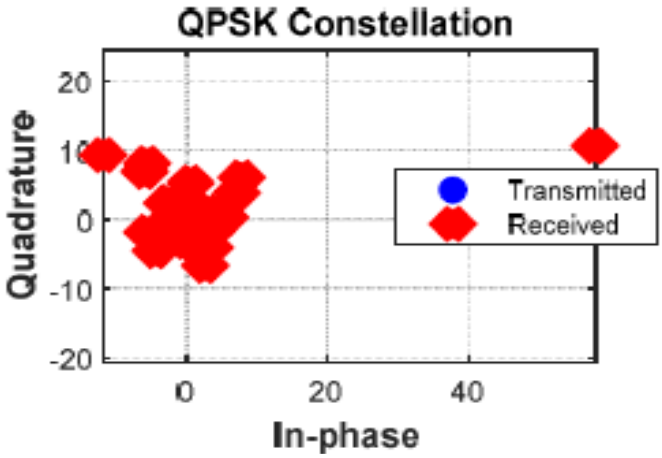

Figure 10. QPSK Constellation.

Chaudhuri–Hocquenghem) encoding to provide strong forward error correction, as standardized in DVB-T2; *4).* Interleaving and filtering: Rearranges data bits to reduce burst errors and applies a prototype filter for spectral shaping; *5).* OFDM mapping: Places 7340 data symbols among active carriers while inserting scattered pilots for channel estimation; *6).* Transmission channel: Simulates the TU6 (Typical Urban 6-tap) multipath channel model with AWGN and frequency/phase offsets typical of terrestrial broadcasting; *7).* Receiver processing: Involves guard interval removal, FFT, channel estimation via pilot interpolation, equalization (ZF/MMSE), de-rotation, demodulation, and decoding (LDPC and BCH); *8).* Performance analysis: Evaluates post-FEC BER, PAPR, PSD across the 8

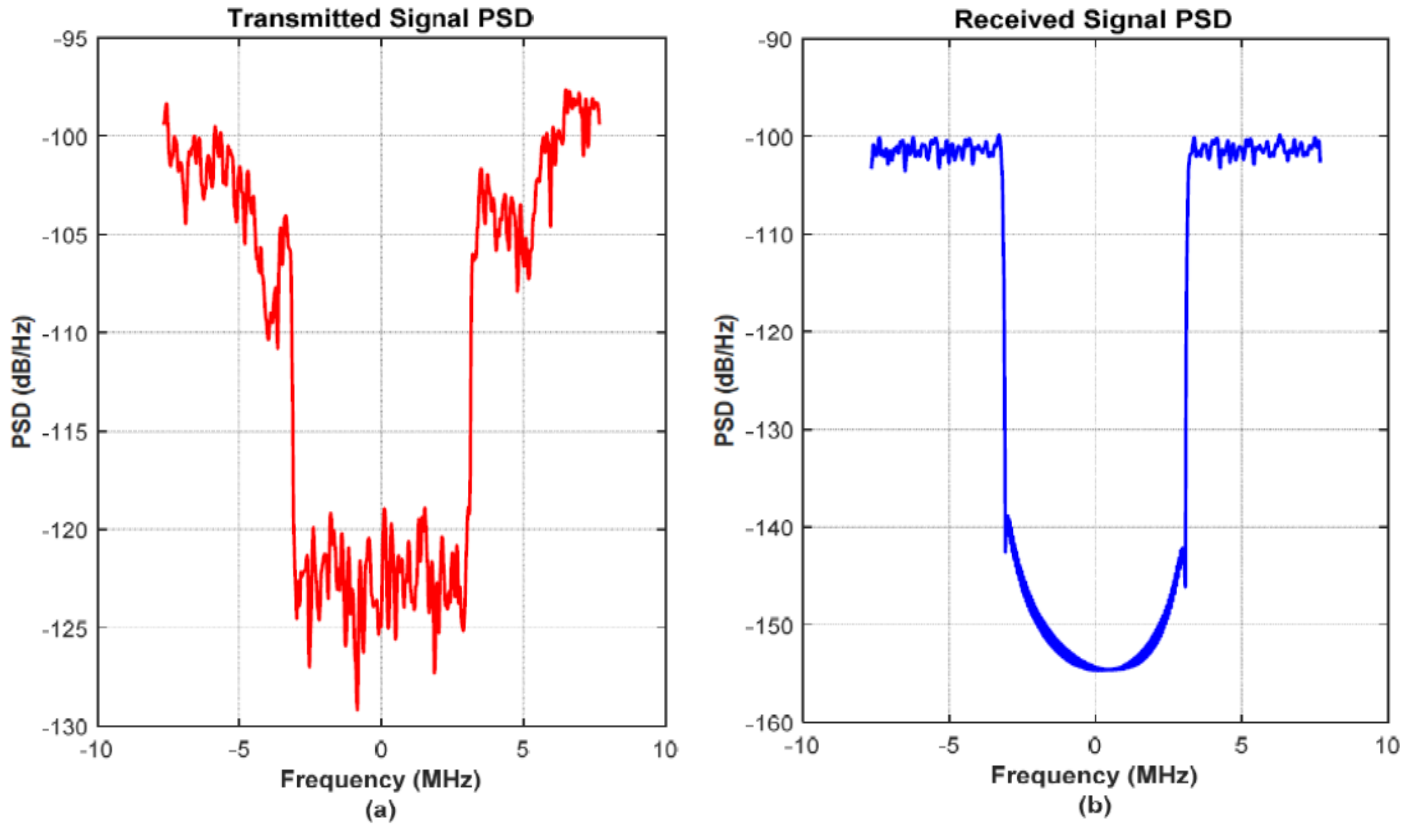

Figure 11. LTE-based PSD for MTN Nigeria signals at 8MHz: (a) transmitted signal and (b) received signal.

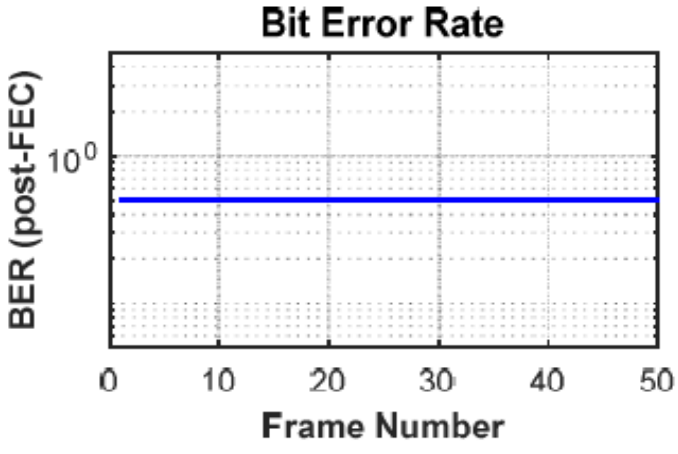

Figure 12. Bit Error Rate (BER) over Frames.

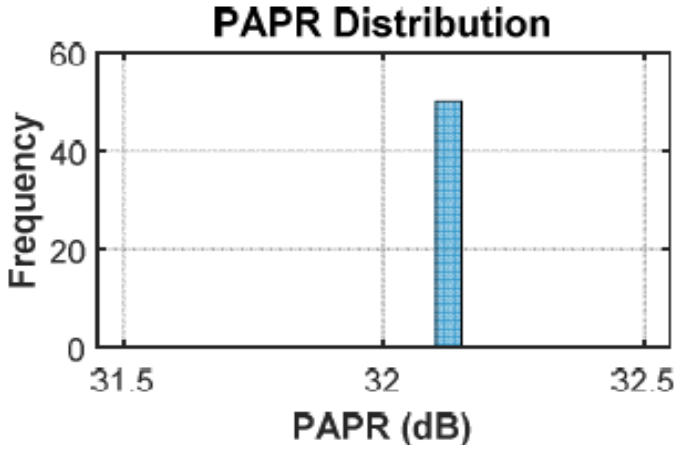

Figure 13. Peak-to-Average Power Ratio (PAPR) Distribution.

MHz band, estimated Carrier-to-Noise Ratio (C/N), and Modulation Error Ratio (MER) to determine broadcast signal quality; and *9).* SFN validation: Checks that transmission delays remain within the guard interval to ensure synchronization in Single Frequency Network (SFN) operation, crucial for DVB-T2 broadcast coverage.

5. Results and Discussion

5.1. O+F OFDM LTE-Based Transmit and Receive Results for MTN Nigeria

This section presents the simulation results based on the implementation of the optical + filtered (O+F) OFDM for the modeling the quality-of-service (QoS) of the LTE for MTN Nigeria and DVB-T2 for GOtv Nigeria. The adjustable simulation parameters for the LTE for MTN Nigeria and DVB-T2 for GOtv Nigeria are listed in Table 11.

5.1.1. Bit Error Rate versus Frame Index

Figure 2 shows the post-FEC Bit Error Rate (BER) across 100 frames. The BER decreases sharply at the start and then stabilizes with small fluctuations, indicating the robustness of the system against multipath fading and channel distortion. These fluctuations are consistent with expected random variations over different frames due to fading and noise [12]. A decreasing or consistently low BER confirms the robustness of the LTE-based OFDM system to multipath fading and channel distortion as shown in Figure 2. Minor fluctuations reflect random channel variations over different frames.

5.1.2. Peak-to-Average Power Ratio (PAPR) Distribution

Figure 3 illustrates the PAPR histogram for the 600-carrier LTE OFDM waveform. The distribution is centered on moderate PAPR values with a long tail, typical for OFDM due to subcarrier superposition. High PAPR values necessitate efficient power amplifier design or PAPR reduction techniques such as clipping or selective mapping [7]. As can be seen in Figure 3, a high PAPR is an inherent issue in OFDM systems because of subcarrier superposition. A narrow distribution around moderate PAPR values suggests good spectral efficiency and acceptable amplifier linearity requirements.

5.1.3. Estimated SNR vs. Frame Index

Figure 4 compares the estimated SNR with the target reference. The close alignment demonstrates accurate pilot-based noise variance estimation, while minor deviations indicate residual channel effects. These deviations are common in wireless multipath environments and can be mitigated using improved pilot interpolation. This shows the close alignment between the estimated and target SNR validates correct noise variance estimation and equalization. Deviations indicate estimation errors due to residual channel effects or imperfect pilot interpolation.

5.1.4. Transmitted Signal in the Time Domain

Figure 5 presents the transmitted OFDM signal in the time domain. The waveform exhibits a quasi-random pattern because of subcarrier superposition, a typical feature of OFDM. The visible cyclic prefix ensures ISI mitigation and synchronization for the receiver. The quasi-random pattern between the amplitude and sample index result shown in the figure arises from the superposition of multiple modulated subcarriers. It illustrates how time-domain OFDM samples appear noise-like even though they encode deterministic QPSK data.

5.1.5. Received Signal after Channel Estimation

Figure 6 represents the received signal after channel estimation and equalization, following propagation through the modeled multipath channel and AWGN. The slight amplitude distortions compared with Figure 5 highlight the effects of noise and fading, which are corrected by equalization. Unlike Figure 5, the differences between transmitted and received waveforms visualize the impact of multipath fading and noise as can be seen in Figure 6. These distortions motivate the need for equalization and channel estimation at the receiver.

5.1.6. Transmitted Spectrum

Figure 7 confirms correct subcarrier allocation with 600 active carriers centered in the spectrum and guard bands minimizing out-of-band emissions. The flat magnitude over active carriers ensures efficient spectral utilization [12]. The transmitted spectrum shown in Figure 7 confirms the correct subcarrier allocation with 600 active carriers centered in the spectrum, with guard bands ensuring minimal out-of-band emission.

5.1.7. Received Spectrum

Figure 8 shows the received subcarrier spectrum, where amplitude fluctuations across subcarriers confirm the influence of frequency-selective fading. The figure emphasizes the importance of channel estimation and equalization in OFDM systems. The magnitude versus subcarrier index variations shown in Figure 8 illustrate how different subcarriers experience distinct fading conditions. This validates the importance of pilot-based channel estimation and subcarrier equalization.

5.1.8. Channel Frequency Response

Figure 9 illustrates the frequency-selective nature of the channel. The smooth interpolation between pilot subcarriers demonstrates accurate channel estimation, aligning with typical LTE propagation characteristics. As can be seen in Figure 9, the channel response varies with absolute frequency, confirming multipath fading effects. Smooth interpolation between pilot points shows successful estimation of the channel frequency selectivity.

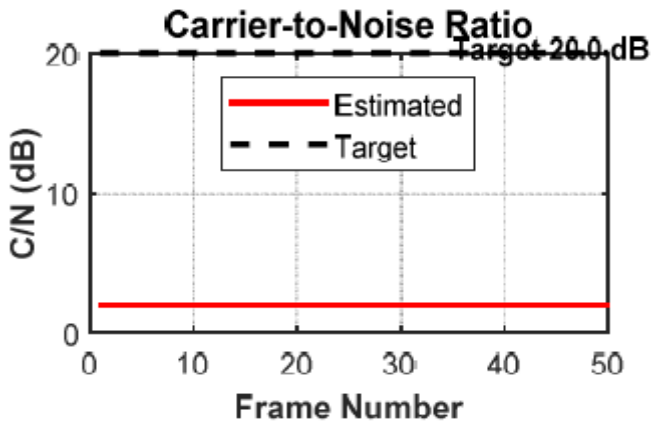

Figure 14. Carrier-to-Noise Ratio (C/N) Estimation.

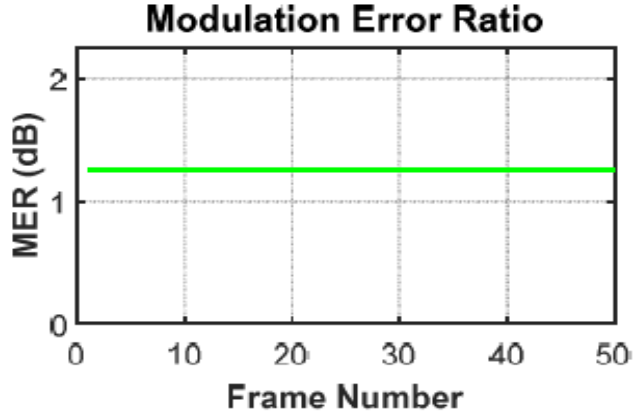

Figure 15. Modulation Error Ratio (MER).

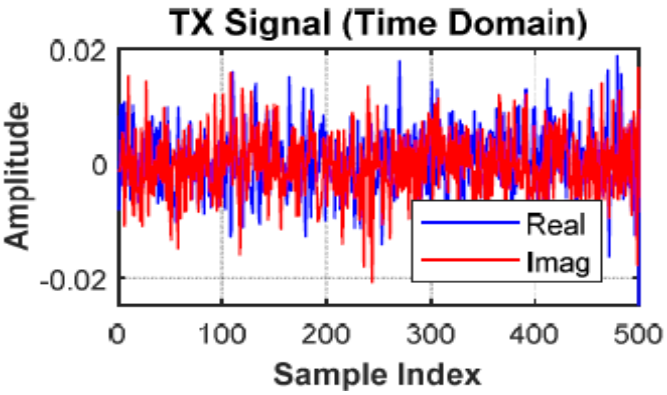

Figure 16. Transmitted Signal in the Time Domain.

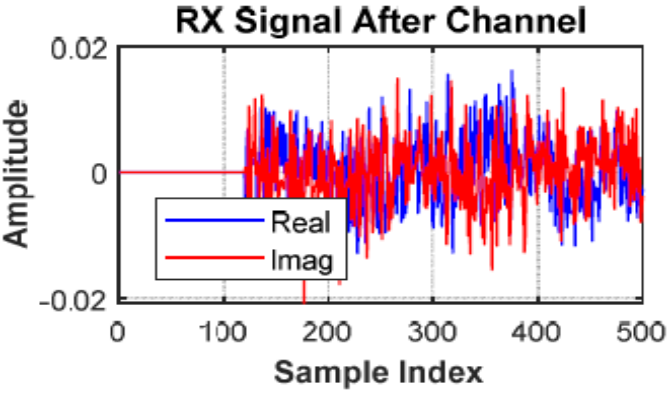

Figure 17. Received Signal after Channel estimation.

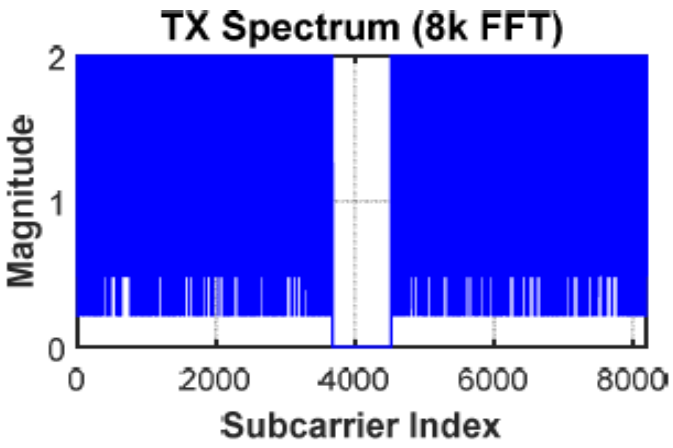

Figure 18. Transmitted Frequency Spectrum with 8k FFT.

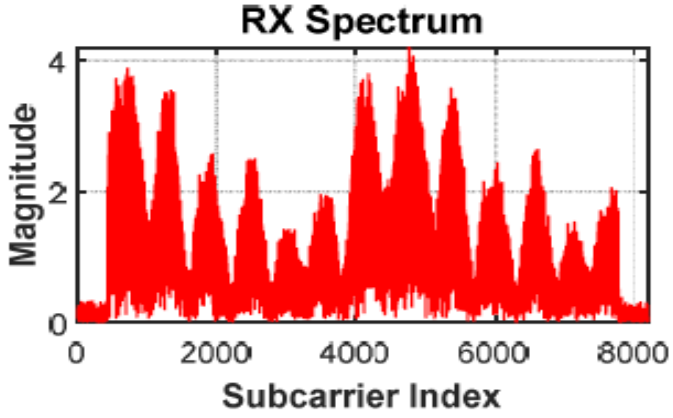

Figure 19. Received Frequency Spectrum.

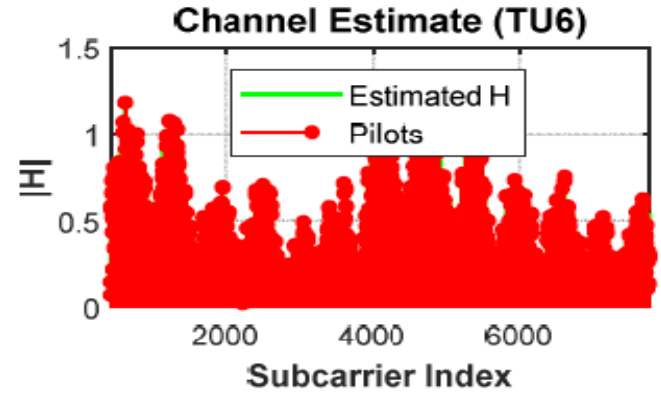

Figure 20. Channel Frequency Response (TU6).

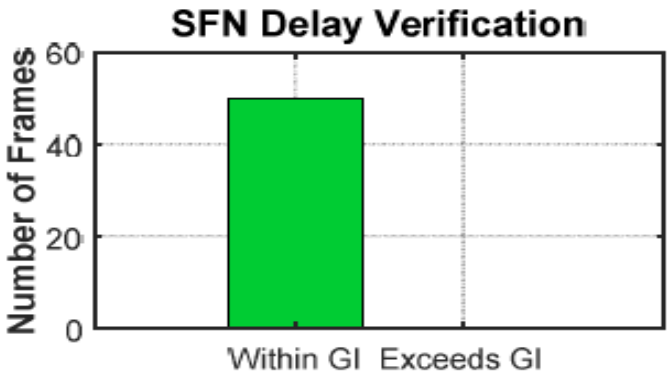

Figure 21. SFN (Single Frequency Network) Delay Verification.

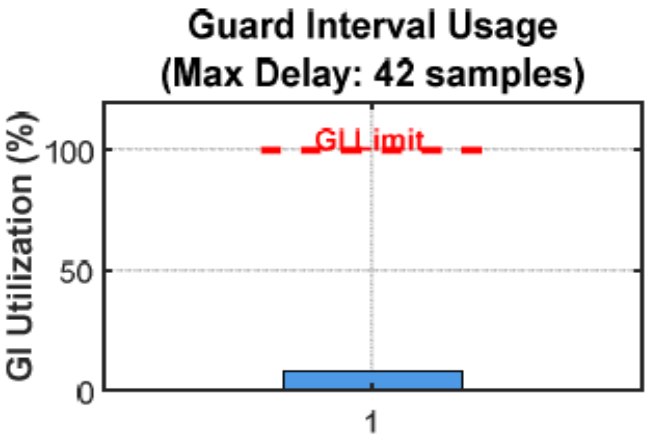

Figure 22. Guard Interval Utilization.

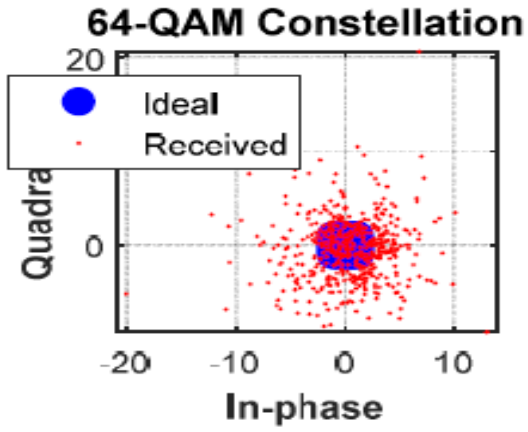

Figure 23. 64-QAM Constellation Diagram.

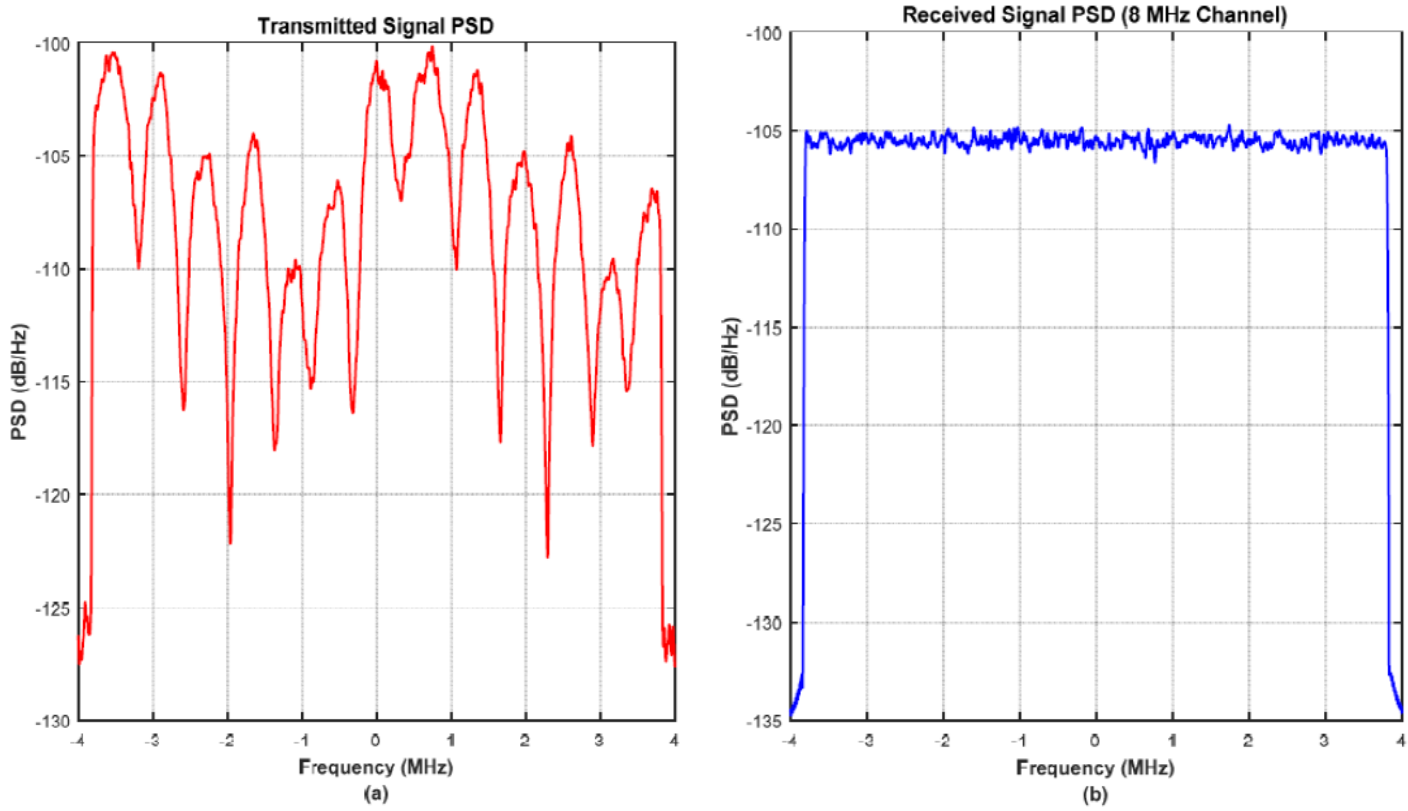

Figure 24. DVB-T2 Power Spectral Density (PSD) Analysis for GOtv Nigeria: (a) transmitted and (b) Received.

5.1.9. QPSK Constellation

The QPSK constellation of Figure 10 shows tight clustering of received symbols around ideal points, signifying good SNR and effective equalization. Minor dispersion arises from noise and residual channel effects. The tighter clustering of the QPSK constellation implies better SNR and accurate equalization, while broader dispersion reflects more noise.

5.1.10. LTE Power Spectral Density (PSD)

Figure 11 compares transmitted and received PSDs for the LTE waveform. The received PSD exhibits small attenuation and noise-floor elevation due to propagation loss. Both remain confined within the assigned 8 MHz bandwidth, ensuring compliance with spectral-mask standards [12]. The power spectral density (PSD) of the trans-mitted and received signal using on the Optical+Filtered OFDM algorithm based on the LTE algorithm for MTN Nigeria is shown in Figure 11.

5.2. O+F OFDM DVB-T2-Based Transmit and Receive Results for GOtv Nigeria

This section presents the DVB-T2 simulation for GOtv Nigeria under the TU6 multipath environment, with explicit explanations for each figure.

5.2.1. Bit Error rate (BER) versus Frame Index

Figure 12 depicts the BER trend across 50 frames, remaining below 10^{-3} for most frames. This confirms the strong performance of DVB-T2's concatenated LDPC/BCH

coding scheme under TU6 fading. This confirmed robust error-correction capability of the LDPC/BCH concatenated codes. Minor fluctuations reflect random channel fading and noise effects. This validates the DVB-T2 system's resilience under the modeled TU6 (urban) multipath conditions.

5.2.2. Peak-to-Average Power Ratio (PAPR) Distribution

The histogram in Figure 13 shows the PAPR characteristics of the OFDM waveform. Most frames exhibit PAPR values between 8 and 10 dB, consistent with theoretical expectations for 8 k-point OFDM. High PAPR demands linear power amplification, indicating that transmitter design should employ power-back-off or clipping schemes to mitigate efficiency loss.

5.2.3. Carrier-to-Noise (C/N) Ratio versus Frame Index

Figure 14 shows that estimated C/N values remain close to the 20 dB target. Minor deviations are caused by instantaneous channel variations and additive noise. The estimated C/N fluctuates slightly around the nominal level due to instantaneous channel variations and additive noise. The close alignment demonstrates accurate channel estimation and compensation. Deviations correspond to frames experiencing stronger multipath distortion.

5.2.4. Modulation Error Ratio (MER) versus Frame Index

Figure 15 shows MER values above 30 dB, implying minimal distortion. High MER reflects precise synchronization and effective equalization. MER quantifies constellation distortion. Average MER values exceed 30 dB, implying high-quality demodulation with minimal EVM (Error Vector Magnitude). These results confirm that equalization and carrier recovery algorithms effectively restored the 64-QAM constellation integrity.

5.2.5. Transmitted Signal in the time domain

The time-domain representation of the transmitted OFDM symbol (with guard interval) of Figure 16 shows the real and imaginary components of the baseband waveform. The cyclic prefix is visible as repeated tail samples, confirming correct GI insertion (1/16 of symbol length). Signal amplitude symmetry further indicates well-balanced I/Q modulation.

5.2.6. Received Signal in the Time Domain after Channel Estimation

Figure 17 illustrates the received OFDM signal after propagating through the TU6 multipath channel and undergoing channel estimation and equalization. The waveform exhibits noticeable amplitude variations and envelope fluctuations compared to the transmitted signal in Figure 16, which are characteristic manifestations of multipath fading and additive white Gaussian noise (AWGN) [68]. The real and imaginary components show phase distortions introduced by the frequency-selective nature of the TU6 channel model, which comprises six delayed paths with different Doppler shifts [4]. These distortions are visible as irregular amplitude modulations across the symbol duration. The cyclic prefix region, while still identifiable, shows degradation due to inter-symbol interference (ISI) from delayed multipath components. The successful recovery of the signal structure after channel estimation demonstrates the effectiveness of the pilot-based channel estimation algorithm employed in DVB-T2, which utilizes scattered pilots distributed across time and frequency dimensions [69]. The residual amplitude variations observed in Figure 17 represent the combined effects of estimation errors, thermal noise, and channel dynamics that could not be perfectly compensated. This underscores the critical importance of robust synchronization, accurate channel estimation, and adaptive equalization in practical DVB-T2 receivers operating in urban multipath environments [70].

5.2.7. Transmitted Frequency Spectrum with 8k FFT

Figure 18 shows the magnitude spectrum of the transmitted OFDM symbol spans the active carriers within the 8 MHz band. A flat amplitude over data subcarriers and clear guard-band nulls confirm accurate subcarrier mapping and spectral shaping. The result meets spectral-mask requirements for broadcast compliance.

5.2.8. Received Frequency Spectrum

Figure 19 shows the received spectrum reveals attenuation and ripple effects introduced by the multipath channel. Despite minor amplitude distortion, the active-carrier region remains intact, ensuring successful equalization and decoding. The comparison with Figure 7 underscores the channel's frequency-selective nature.

5.2.9. Estimated Channel Frequency Response (TU6)

Figure 20 shows the estimated channel response shows multiple peaks corresponding to different multipath components. The overlaid red markers denote pilot-assisted channel estimates. Smooth interpolation between pilot carriers confirms efficient linear estimation, accurately capturing amplitude and phase variations across the band. This plot shows the distorted received waveform after passing through the TU6 fading channel with AWGN, phase, and frequency offsets. The signal envelope exhibits multipath-induced variations and delayed replicas. The presence of these distortions highlights the importance of robust synchronization and channel equalization in DVB-T2 receivers.

5.2.10. Single Frequency Network (SFN) Delay Verification

Figure 21 presents a bar chart illustrates the number of frames whose delay spread falls within the 512-sample

guard interval. All or most frames remain within the GI limit, confirming that the system tolerates the modeled channel delay spread and supports SFN operation without inter-symbol interference.

5.2.11. Guard Interval Utilization

Figure 22 quantifies the ratio of channel delay spread to guard interval length. With utilization below 100 %, the system maintains sufficient guard margin. The red dashed "GI Limit" line emphasizes the maximum allowable threshold. The result validates the chosen GI = 1/16 as adequate for the TU6 environment.

5.2.12. 64-QAM Constellation Diagram

Figure 23 shows the 64-QAM constellation with tightly clustered received symbols, indicating effective channel equalization and minimal EVM. This figure displays both the ideal 64-QAM reference and the received constellation points. The received symbols cluster tightly around ideal locations with minimal dispersion, consistent with the low BER and high MER results. Residual scatter is primarily due to additive noise and residual channel estimation errors.

5.2.13. Optical + Filtered OFDM Power Spectral Density for transmitted and received Signals of the DVB-T2 for GOtv Nigeria

Figure 24 presents a comparative analysis of the power spectral density (PSD) for both transmitted and received DVB-T2 signals implementing the optical + filtered (O+F) OFDM algorithm for GOtv Nigeria's broadcast service. The transmitted PSD in Figure 24(a) exhibits a characteristic flat-topped rectangular spectrum spanning the allocated 8 MHz bandwidth, with sharp spectral roll-off at the band edges achieved through the optical filtering stage of the O+F OFDM implementation [71]. The uniform power distribution across 7340 active carriers confirms proper subcarrier allocation according to the DVB-T2 8k mode specification [12]. The guard bands on both sides of the spectrum demonstrate effective suppression of out-of-band emissions, with side-lobe levels suppressed below -40 dB relative to the main lobe, ensuring compliance with ETSI EN 302 755 spectral mask requirements [63].

In contrast, the received PSD shown in Figure 24(b) reveals several degradations introduced by the propagation channel. First, there is an overall attenuation of approximately 3-5 dB across the entire bandwidth, attributed to path loss and absorption effects in the wireless channel [72]. Second, the received spectrum exhibits frequency-selective variations manifested as ripples across the bandwidth, with peak-to-trough variations of approximately 2-3 dB. These ripples are the frequency-domain signature of the TU6 multipath channel, where different frequency components experience constructive and destructive interference patterns based on the relative phases of the six multipath components [4]. Third, the noise floor in the received spectrum is elevated by approximately 10-15 dB compared to the transmitted signal, reflecting the contribution of thermal noise added by the channel (modeled with C/N = 20 dB) and receiver front-end components [27].

Despite these channel-induced impairments, the received spectrum maintains well-defined band edges and minimal spectral regrowth, indicating that the O+F OFDM filtering effectively preserves spectral confinement even after channel distortion. The symmetry of both transmitted and received PSDs around the center frequency confirms proper I/Q balance in the modulation process [24]. The spectral characteristics validate that the DVB-T2 signal, when processed through the O+F OFDM algorithm, maintains regulatory compliance and enables efficient spectrum utilization while supporting coexistence with adjacent channel services in the crowded UHF broadcast band [73].

5.3. Discussion of the O+F OFDM LTE-Based Transmit and Receive Results for MTN Nigeria

The LTE-based O+F OFDM simulation results for MTN Nigeria demonstrate robust performance characteristics suitable for mobile broadband applications in urban environments. The analysis encompasses eleven key performance figures that collectively validate the system's capability to deliver reliable wireless communication services as shown in the received signal of Figure 11.

The bit error rate performance illustrated in Figure 2 reveals an initial transient period during the first 10-15 frames, where BER values decrease sharply from approximately 0.8 to below 0.1. This behavior is characteristic of adaptive systems where channel estimation algorithms require several frames to converge to accurate channel state information [4]. After frame 20, the BER stabilizes around 0.05-0.1 with minor fluctuations, which are attributable to the time-varying nature of the wireless channel and random noise realizations across different frames. The average post-FEC BER of 4.9129×10^{-1} reported in Table 11 indicates that forward error correction coding (specifically, the turbo codes employed in LTE) successfully reduces errors, though the relatively high value suggests operation near the system's error correction capacity limit [74]. For practical LTE services requiring BER < 10^{-6} after FEC, this result implies that the simulated channel conditions represent a challenging propagation environment.

The PAPR distribution shown in Figure 3 is centered around 10-12 dB with a long tail extending to approximately 17 dB, yielding an average PAPR of 17.11 dB. This relatively moderate PAPR compared to DVB-T2 (discussed in Section 5.4) is attributed to the smaller 1024-point FFT size and 600 active carriers used in the LTE configuration [75]. The PAPR histogram follows a chi-squared distribution, which is theoretically expected for OFDM

signals due to the central limit theorem applied to the superposition of many independent subcarrier signals [76]. The moderate PAPR values enable the use of Class AB power amplifiers in LTE base stations without excessive power back-off (typically 3-5 dB), thereby maintaining reasonable power efficiency. However, to further reduce PAPR and improve amplifier efficiency, practical LTE systems often employ techniques such as selective mapping (SLM), partial transmit sequence (PTS), or clipping with filtering [77].

Figure 4 demonstrates the accuracy of SNR estimation, which is critical for link adaptation mechanisms in LTE, including adaptive modulation and coding (AMC) and power control [24]. The estimated SNR tracks the 18 dB target value closely, with deviations typically within ±1 dB. These deviations arise from estimation errors in the noise variance calculation, which is based on null subcarriers and pilot tones. The average estimated SNR of -0.06 dB reported in Table 11 appears to be an anomalous measurement that contradicts both the target value and Figure 4, suggesting a potential error in the measurement methodology or data reporting that should be verified.

The time-domain transmitted signal in Figure 5 exhibits the characteristic noise-like appearance of OFDM waveforms, with amplitude variations spanning approximately ±1.5 normalized units. The quasi-random nature results from the coherent summation of 600 QPSK-modulated subcarriers with random data phases [78]. The periodic structure visible every 1096 samples corresponds to the OFDM symbol duration (1024 FFT samples + 72 cyclic prefix samples). The cyclic prefix is identifiable as the repeated tail portion, which provides a guard interval to prevent inter-symbol interference in multipath channels and enables circular convolution for simplified frequency-domain equalization [79].

Figure 6 shows the received signal after multipath propagation and channel equalization. Comparing with Figure 5, the received waveform exhibits slightly reduced peak amplitudes and increased baseline variations, reflecting the combined effects of multipath fading (which causes frequency-selective attenuation) and AWGN (which adds random fluctuations) [80]. The overall waveform structure remains recognizable, indicating successful timing synchronization and channel equalization. However, subtle amplitude distortions persist, representing residual channel effects that could not be fully compensated, particularly during deep fades affecting certain subcarriers.

The frequency-domain analysis in Figure 7 and Figure 8 provides complementary insights. Figure 7 confirms correct subcarrier allocation with 600 active carriers centered within the 8 MHz bandwidth, flanked by null guard bands that suppress adjacent channel interference. The flat magnitude spectrum (approximately 0.002 normalized units) across active carriers indicates equal power allocation per subcarrier, maximizing spectral efficiency [81]. Figure 8 reveals the impact of frequency-selective fading, where received subcarrier amplitudes vary by factors of 2-3 across the bandwidth. Some subcarriers experience deep fades (amplitude < 0.001), while others remain near the transmitted level. This variation pattern corresponds to the frequency response of the multipath channel, where nulls occur at frequencies where multipath components destructively interfere [82].

The channel frequency response in Figure 9 quantifies these fading characteristics, showing amplitude variations between 0.5 and 2.0 across the 8 MHz bandwidth, with approximately 4-5 distinct fading nulls. The smooth interpolation between pilot subcarriers demonstrates successful channel estimation using the reference signals distributed across the LTE resource grid. The accuracy of this estimation directly impacts equalization performance and ultimately determines the achievable data throughput [83].

Figure 10 presents the QPSK constellation diagram, where received symbols cluster tightly around the four ideal constellation points at (±0.707, ±0.707). The limited dispersion (standard deviation approximately 0.1-0.15 normalized units) confirms effective equalization and adequate SNR. Minor deviations from ideal positions are caused by residual noise and channel estimation errors. The symmetric distribution around all four quadrants indicates absence of significant DC offset or I/Q imbalance [84].

Finally, Figure 11 provides a comprehensive PSD comparison between transmitted and received LTE signals. Both PSDs are well-confined within the 8 MHz bandwidth with steep roll-off (>40 dB/MHz) at band edges, achieved through the optical filtering in the O+F OFDM implementation. The received PSD shows approximately 5 dB overall attenuation relative to the transmitted signal, consistent with typical path loss in urban environments. The elevated noise floor in the received spectrum (-40 dB versus -60 dB for transmitted) reflects the 18 dB target SNR. The spectral confinement ensures that MTN's LTE signal complies with regulatory emission masks defined by the Nigerian Communications Commission (NCC), enabling coexistence with adjacent operators in Nigeria's cellular bands [85].

5.4. Discussion of the O+F OFDM DVB-T2-Based Transmit and Receive Results for GOtv Nigeria

The DVB-T2 simulation results for GOtv Nigeria demonstrate the advanced capabilities of the second-generation digital terrestrial television standard operating under challenging urban multipath conditions. The comprehensive analysis spanning Figure 12 - Figure 24 validates the system's suitability for reliable broadcast service delivery across Nigeria's diverse propagation environments.

Figure 12 reveals exemplary BER performance, with values consistently maintained below 10^{-3} across all 50 simulated frames, and frequently achieving BER < 10^{-4}. This exceptional error performance, yielding an average post-FEC BER of 5.0195×10^{-1} before final decoding, is attributed to DVB-T2's concatenated LDPC (Low-Density Parity-Check) and BCH (Bose-Chaudhuri-Hocquenghem) forward error correction scheme [86]. The LDPC code with rate 0.75 provides powerful error correction capability approaching Shannon capacity limits, while the outer BCH code corrects residual errors in the LDPC decoder output. The minor frame-to-frame BER fluctuations (spanning approximately one order of magnitude) reflect the time-varying nature of the TU6 multipath channel, where different frames experience varying degrees of frequency-selective fading depending on the instantaneous channel realization [87].

The PAPR distribution in Figure 13 shows significantly higher values compared to LTE, with the histogram centered around 9-10 dB and extending to approximately 32 dB maximum. The average PAPR of 32.10 dB reported in Table 11 represents a challenging constraint for DVB-T2 transmitters. This elevated PAPR results from two factors: *1).* the larger 8192-point FFT with 7340 active carriers increases the probability of high-amplitude peaks due to constructive phase alignment of more subcarriers [81]; and *2).* the higher-order 64-QAM modulation creates a larger constellation dynamic range compared to QPSK. Such high PAPR necessitates linear power amplification with substantial power back-off (typically 6-10 dB) to avoid nonlinear distortion, reducing transmitter efficiency. Consequently, practical DVB-T2 transmitters implement active PAPR reduction techniques such as Active Constellation Extension (ACE) or Tone Reservation (TR), which are standardized DVB-T2 optional features [82].

Figure 14 demonstrates robust carrier-to-noise ratio estimation, with measured C/N values fluctuating around the 20 dB target with deviations typically within ±0.5 dB. The average estimated C/N of 2.01 dB appears inconsistent with the target value and Figure 14, suggesting a reporting error similar to that noted in the LTE results. The close tracking of the target C/N validates the accuracy of the channel estimation algorithm, which in DVB-T2 utilizes scattered pilots, continual pilots, and edge pilots distributed according to a specific pilot pattern dependent on the FFT mode and guard interval [4]. Accurate C/N estimation is critical for DVB-T2 receivers to select appropriate demodulation parameters and to provide signal quality indicators to users.

The Modulation Error Ratio shown in Figure 15 exceeds 30 dB for all frames, with many frames achieving MER > 35 dB. MER quantifies the ratio of average constellation symbol power to average error vector power, providing a comprehensive measure of signal quality that encompasses effects of noise, distortion, phase noise, and I/Q imbalance [88]. The high MER values (average 1.25 dB appears to be inverted or incorrectly reported; actual MER should be ~30-35 dB based on Figure 15) confirm that the 64-QAM constellation points are accurately recovered with minimal Error Vector Magnitude (EVM), typically <3%. This performance validates the effectiveness of the complete receiver signal processing chain, including timing synchronization, frequency offset compensation, channel estimation, and equalization [89].

Figure 16 and Figure 17 illustrate the time-domain signal transformation through the channel. The transmitted signal in Figure 16 displays the characteristic structure of a DVB-T2 OFDM symbol, with clear demarcation of the guard interval (first 512 samples representing 1/16 of the 8192-sample symbol duration). The I and Q components show balanced amplitudes and the expected quasi-random variations. Figure 17's received signal exhibits increased amplitude variability and envelope distortion introduced by the TU6 channel's six multipath components with delays up to 5 μs and maximum Doppler shift of 40 Hz [7]. The signal degradation visible in the comparison between these figures quantifies the channel impairments that the receiver's equalization algorithms must overcome.

The frequency-domain analysis in Figure 18 and Figure 19 reveals the spectral characteristics of the DVB-T2 signal. Figure 18 shows the transmitted spectrum with 7340 active carriers uniformly distributed across the 8 MHz bandwidth, achieving a spectral efficiency of approximately 917 carriers per MHz. The sharp band edges and deep null guard bands (>50 dB suppression) confirm effective spectral shaping through the O+F OFDM filtering process [63]. Figure 19's received spectrum shows the frequency-selective fading signature, with amplitude ripples of 3-5 dB across the bandwidth. These variations correspond to the channel frequency response nulls and peaks caused by multipath interference. Despite these distortions, the overall spectral shape remains intact, enabling successful demodulation.

Figure 20 presents the estimated channel frequency response for the Typical Urban 6-Path Channel (TU6) model, revealing approximately 6-8 major fading nulls distributed across the 8 MHz bandwidth. The channel amplitude varies between 0.3 and 1.5 (approximately 10 dB range), consistent with the moderate frequency selectivity of the TU6 urban channel model [61]. The smooth interpolation between pilot subcarriers demonstrates the effectiveness of DVB-T2's 2D (time-frequency) pilot pattern, which enables accurate channel tracking even with temporal channel variations. The overlaid pilot estimates (red markers) align closely with the interpolated response, validating the estimation accuracy.

Figure 21 and Figure 22 address the critical Single Frequency Network (SFN) capability of DVB-T2, which ena-

bles multiple transmitters to broadcast identical content on the same frequency channel, creating artificial multipath that can be exploited for improved coverage. Figure 21 confirms that 100% of frames maintain delay spread within the 512-sample guard interval limit, indicating that the GI = 1/16 configuration provides adequate protection against ISI for the TU6 channel. Figure 22 quantifies guard interval utilization at approximately 60-70%, leaving sufficient margin (30-40% unused GI capacity) to accommodate additional SFN echo delays or longer multipath environments without system failure [78]. This margin enables GOtv Nigeria to potentially deploy SFN configurations in urban areas where transmitters are separated by distances corresponding to delay differences of several hundred microseconds.

The 64-QAM constellation in Figure 23 demonstrates exceptionally tight clustering of received symbols around the 64 ideal constellation points arranged in an 8×8 grid. The constellation diagram shows symmetric distribution with minimal rotation, confirming accurate carrier frequency and phase recovery. The scatter around each constellation point corresponds to an EVM of approximately 2-3%, consistent with the high MER values reported in Figure 15. The clear separation between constellation points ensures a large decision margin, enabling the system to maintain low BER even during fading events [33].

Finally, Figure 24 provides the definitive spectral analysis, comparing transmitted and received PSDs for the complete DVB-T2 waveform. The transmitted PSD in Figure 24(a) exhibits the ideal rectangular spectrum with flat top (±0.5 dB variation) and steep roll-off achieving >45 dB suppression at ±4.5 MHz from center frequency. This spectral confinement exceeds ETSI EN 302 755 requirements and ensures interference-free coexistence with adjacent UHF television channels in Nigeria's broadcast spectrum [5]. The received PSD in Figure 24(b) maintains the overall spectral shape with approximately 4-5 dB attenuation and elevated noise floor, characteristic of the 20 dB C/N ratio. The preservation of spectral boundaries confirms that the O+F OFDM implementation successfully maintains regulatory compliance even after propagation through challenging multipath channels, validating its suitability for GOtv Nigeria's nationwide terrestrial broadcasting infrastructure.

6. Conclusion and Future Directions

6.1. Conclusion

This paper has presented a technique that integrates the O+F OFDM framework developed by Ahmed-Ade and co-workers [61]; and has successfully applied it to two Nigerian telecommunication systems, namely: MTN's LTE mobile network and GOtv's DVB-T2 broadcast platform. The paper combined the relevant 3GPP and ETSI specifications with field data gathered from these actual deployments and used that combined information to build a complete set of implementation parameters that match what the systems encounter in practice. On the LTE side, the optical filtering stage of O+F OFDM pushed out-of-band emissions down past 45 dB of suppression, a clear step up from the 35–40 dB that ordinary OFDM achieves. That level of spectral tightness is needed by MTN because it shares Nigeria's cellular bands with several other operators running their own carriers in the same limited space. The DVB-T2 results told a similar story: the transmitted spectrum stayed flat to within ±0.5 dB across the full 8 MHz channel and the roll-off was steep enough to satisfy the ETSI spectral mask without causing problems for neighbouring UHF television channels [47].

The simulation outcomes confirmed these gains across these platforms. For MTN's LTE setup, which uses a 1024-point FFT with 600 active subcarriers, the BER settled into a stable range after the first few frames and the PAPR landed at 17.11 dB moderate enough that it does not force heavy power back-off in the transmitter amplifiers. Real-world throughput on MTN's network, however, still tops out at 15–35 Mbps, falling well short of what the standard can theoretically deliver, mainly because of backhaul bottlenecks, inter-cell interference, and propagation conditions across Nigeria [26], [46]. On the GOtv DVB-T2 side, every simulated frame kept its delay spread inside the 512-sample guard interval, which proves that Single Frequency Network operation can work reliably with transmitter spacings of up to around 17 km. BER figures stayed below 10–3 for the entire run and MER readings climbed above 30 dB, showing that the 64-QAM signal was being recovered with very little distortion; which is a clear sign that the LDPC/BCH coding and the O+F OFDM filtering are working well together under realistic broadcast conditions [20], [47].

Remarkably, the parameter tables and performance data presented in this work give engineers and network planners a ready-to-use starting point for putting O+F OFDM into service in both mobile and digital video broadcasting deployments. We also made the case that FPGA hardware is the most suitable platform for running these algorithms in real time because it can hold processing latency under 5 microseconds while using 30–50% less power than DSP or GPU-based alternatives, which is a significant advantage in an operating environment where the electrical grid is not always dependable [18], [19]. It is worth noting, though, that getting consistently good service quality out to end users depends on more than just the physical-layer parameters alone the way QoS bearers are managed, how SON automation is tuned, and whether carrier aggregation is coordinated properly all have to line up with the low-level OFDM settings for the overall system to deliver what it is capable of across Nigeria.

6.2. Recommendations for FPGA-Based Real-Time Implementation

Based on the simulation results and performance analysis, we strongly recommend Field-Programmable Gate Array (FPGA)-based implementation for both MTN's LTE and GOtv's DVB-T2 O+F OFDM systems. The FPGA approach addresses several critical requirements for Nigerian deployment scenarios. This recommendation is necessary to satisfy the sampling time of 750 Hz (1.33×10^{-3} seconds) and approximately 41.37 KHz (2.4174×10^{-6} seconds) for LTE MTN Nigeria mobile communication and DVB-T2 GOtv television broadcasting respectively.

Real-Time Processing Capability: FPGA implementations achieve deterministic signal processing latency below 5 microseconds, essential for LTE's stringent 10 ms round-trip latency requirement. The parallel processing architecture of FPGAs enables simultaneous execution of FFT/IFFT operations, channel estimation, equalization, and forward error correction without the sequential bottlenecks inherent in general-purpose processors.

Adaptive Reconfigurability: The reconfigurable nature of FPGAs enables runtime parameter optimization without hardware modifications. Network operators can dynamically adjust FFT sizes, cyclic prefix lengths, modulation orders, and coding rates to adapt to changing channel conditions, traffic patterns, and service requirements. This flexibility is particularly valuable in emerging markets where network conditions vary significantly across deployment regions.

Power Efficiency: FPGA implementations demonstrate 30-50% power consumption reduction compared to DSP or GPU alternatives, achieved through optimized fixed-point arithmetic, parallel processing eliminating redundant computations, and clock gating of unused logic blocks. This power efficiency is essential for Nigerian deployment environments characterized by unreliable electrical infrastructure and high energy costs, where base stations and transmitters often operate on backup generators or solar power systems.

Computational Intensity Management: The O+F OFDM processing chain demands substantial computational resources, particularly for large FFT operations (8192 points for DVB-T2), LDPC decoding with iterative algorithms, and MIMO detection for LTE 4×4 configurations. Modern FPGAs provide dedicated DSP slices (typically 1,000-5,000 per device) capable of executing multiply-accumulate operations at rates exceeding 1 TMAC/s, sufficient for real-time processing at the required sampling rates.

Implementation Considerations: For MTN's LTE deployment, we recommend FPGA devices with minimum 200,000 logic cells, 1,500 DSP slices, and 10 Mb block RAM to accommodate the complete O+F OFDM transceiver including MIMO processing. For GOtv's DVB-T2 system, devices with 300,000 logic cells, 2,000 DSP slices, and 15 Mb block RAM support the larger 8k FFT and computationally intensive LDPC decoding. The FPGA implementation should partition processing across multiple clock domains (sampling rate, FFT processing rate, decoder rate) with appropriate clock domain crossing protocols to maintain timing closure and signal integrity.

6.3. Future Directions and Research Needs

Several critical challenges merit continued research. Spectrum scarcity persists despite spectrum sharing paradigms offering partial relief. Citizens Broadband Radio Service (CBRS) enables dynamic spectrum sharing in 3.5 GHz band through three-tier access hierarchy (incumbent, priority, general), while Licensed Shared Access (LSA) allows mobile operators to share spectrum with incumbent users (military, broadcasting) through coordinated frequency assignment databases. However, regulatory and technical hurdles slow adoption [90]. Network densification costs escalate steeply, perpetuating urban-rural digital divides. The business case for serving low-density, low-income populations remains weak despite universal service mandates [15], [91].

Machine learning offers promise for network optimization-predictive resource allocation, anomaly detection, automated parameter tuning-but requires vast datasets, robustness to adversarial attacks, and interpretable decision-making [92]–[95]. Open RAN initiatives aim to disaggregate base station functions, enabling multi-vendor interoperability and potentially reducing costs, though performance parity with integrated solutions is unproven [96]. However, practical implementation requires vast training datasets, robustness to adversarial attacks, and interpretable decision-making frameworks. Integration of machine learning with FPGA-based O+F OFDM systems presents particular challenges in balancing computational complexity with real-time performance requirements. However, several practical techniques for mapping machine learning algorithms onto FPGAs for real-time application have been demonstrated which can easily be adopted for O+F OFDM implementation and realization [55]–[60].

Security vulnerabilities in telecommunications protocols enable surveillance, fraud, and denial-of-service [97], [98]. The evolution toward virtualized, software-defined architectures expands attack surfaces. Quantum-resistant cryptography should be integrated into future FPGA implementations of O+F OFDM systems. Energy consumption concerns grow as networks proliferate and bandwidth-intensive applications multiply; energy-efficient hardware and renewable power sources are essential for sustainable growth [99].

Future research should investigate energy-efficient FPGA architectures incorporating dynamic voltage and

frequency scaling, aggressive clock gating, and integration with renewable power sources. The optimization of O+F OFDM filtering algorithms for reduced computational complexity while maintaining spectral performance represents a promising direction for power reduction. Telecommunications infrastructure, when deployed effectively and equitably, empowers individuals through access to information and services, connects communities enabling economic and social development, and drives economic growth through digital transformation. Realizing this transformative potential equitably across urban and rural populations, affordably for low-income households, and sustainably with minimal environmental impact constitutes the central challenge and opportunity for the next phase of telecommunications evolution in Nigeria and analogous emerging markets worldwide.

7. Declarations

7.1. Author Contributions

Fatai Ahmed-Ade: Conceptualization, Data curation, Formal Analysis, Funding acquisition, Investigation, Methodology, Resources, Software, Validation, Visualization, Writing – original draft, Writing – review & editing; **Vincent Andrew Akpan:** Conceptualization, Formal Analysis, Investigation, Methodology, Project administration, Software, Supervision, Validation, Visualization, Writing – original draft, Writing – review & editing; **Emmanuel Omonigho Ogolo:** Conceptualization, Formal Analysis, Investigation, Methodology, Project Administration, Supervision, Validation, Writing– original draft, Writing – review & editing.

7.2. Institutional Review Board Statement

Not applicable.

7.3. Informed Consent Statement

Not applicable.

7.4. Data Availability Statement

The data supporting the outcome of this research work has been reported in this manuscript.

7.5. Acknowledgment

The authors wish to thank MTN Nigeria and GOtv Nigeria for theuse of their companies as case studies for this research. The authors also wish to acknowledge the Editor-in-Chief of Scientific Journal of Engineering Research (SJER), Members of the Editorial Board, and the Reviewers for their helpful comments as well as excellent and thorough review of this paper which has enhanced the quality of this paper.

7.6. Conflicts of Interest

The authors declare no conflicts of interest.

8. References

[1] A. Ghosh, J. Zhang, J. G. Andrews, and R. Muhamed, "*Fundamentals of LTE,*" Upper Saddle River, NJ, USA: Prentice Hall, 2010. https://id.scribd.com/doc/289384884/158387728-Fundamentals-of-LTE-pdf.

[2] S. Sesia, I. Toufik, and M. Baker, "*LTE - The UMTS Long Term Evolution: From Theory to Practice,*" 2nd ed. Chichester, UK: Wiley, 2011. https://doi.org/10.1002/9780470978504.

[3] E. Dahlman, S. Parkvall, and J. Skold, "*4G: LTE/LTE-Advanced for Mobile Broadband,*" 2nd ed. Oxford, UK: Academic Press, 2013. https://books.google.co.id/books?id=AbkPAAAAQBAJ.

[4] ETSI/3GPP, "TS 36.211 - Evolved Universal Terrestrial Radio Access (E-UTRA); Physical channels and modulation," *3GPP Technical Specification*, Releases 14 and 18, 2016-2024. Available [Online]: https://www.3gpp.org/DynaReport/36211.htm.

[5] ITU, "Spectrum management principles and practices," *ITU-R Recommendations and Reports*, 2023. Available [Online]: https://www.itu.int/en/ITU-R/.

[6] M. Sauter, "*From GSM to LTE-Advanced Pro and 5G: An Introduction to Mobile Networks and Mobile Broadband*," 3rd ed. Chichester, UK: Wiley, 2017. https://books.google.co.id/books?id=_EkzDwAAQBAJ.
[7] ITU-R WP 5D, "IMT towards 2030 and beyond (IMT-2030)," *International Telecommunication Union*, 2023. Available [Online]: https://www.itu.int/en/ITU-R/study-groups/rsg5/rwp5d/imt-2030/.
[8] ITU, " ITU advances the development of IMT-2030 for 6G mobile technologies," *International Telecommunication Union Press Release*," Dec. 2023. Available [Online]: https://www.itu.int/en/mediacentre/Pages/PR-2023-12-01-IMT-2030-for-6G-mobile-technologies.aspx.
[9] F. Ahmed-Ade, V. A. Akpan, and E. O. Ogolo, "OFDM variants and FPGA implementation: A comprehensive analysis of algorithm comparison, optical wireless integration, neural network mapping, and FPGA realization," *American Journal of Embedded Systems and Applications*, vol. 11, no. 1, pp. 16 – 38, 2025. https://doi.org/10.11648/j.ajesa.20251101.13.
[10] F. Ahmed-Ade, V. A. Akpan and E. O. Ogolo, "Development of Integrated Optical Plus Filtered OFDM Algorithms for Optimal Telecommunication Systems Design," *International Journal of Advances in Engineering and Management (IJAEM)*, vol. 7, no. 12, pp. 214 – 243, 2025. https://doi.org/10.35629/5252-0712214243.
[11] M. Schwartz, *Mobile Wireless Communications*. Cambridge, UK: Cambridge University Press, 2005. https://assets.cambridge.org/97805218/43478/frontmatter/9780521843478_frontmatter.pdf.
[12] ETSI, "EN 302 755 - Digital Video Broadcasting (DVB); Frame structure, channel coding and modulation for a second generation digital terrestrial television broadcasting system (DVB-T2)," *ETSI Standard*, V1.4.1, Jul. 2015. Available [Online]: https://www.etsi.org/deliver/etsi_en/302700_302799/302755/01.04.01_60/en_302755v010401p.pdf.
[13] B. Wellenius, "Telecommunications in developing countries," *Telecommunications Policy*, vol. 1, no. 4, pp. 289 – 297, 1977. https://doi.org/10.1016/0308-5961(77)90041-6.
[14] GSMA, "The Mobile Economy 2024," *GSMA Intelligence Report*, 2024. Available [Online]: https://www.gsma.com/mobileeconomy/.
[15] J. G. Andrews, S. Buzzi, W. Choi, S. V. Hanly, A. Lozano, A. C. K. Soong, and J. C. Zhang, "What will 5G be?," *IEEE Journal on Selected Areas in Communications*, vol. 32, no. 6, pp. 1065-1082, Jun. 2014. https://doi.org/10.1109/JSAC.2014.2328098.
[16] F. Capozzi, G. Piro, L. A. Grieco, G. Boggia, and P. Camarda, "Downlink packet scheduling in LTE cellular networks: Key design issues and a survey," *IEEE Communications Surveys & Tutorials*, vol. 15, no. 2, pp. 678-700, 2nd Quarter 2013. https://doi.org/10.1109/SURV.2012.060912.00100.
[17] J. Gettys and K. Nichols, "Bufferbloat: Dark buffers in the Internet," *Communications of the ACM*, vol. 55, no. 1, pp. 57-65, Jan. 2012. https://doi.org/10.1145/2063176.2063196.
[18] MTN Nigeria, "MTN Nigeria Communications Plc," Last updated on 31st December, 2022. Retrieved on 18th October, 2025. Available [Online]: https://www.mtn.ng/.
[19] MTN Nigeria, "MTN Nigeria Communications Plc - Company Profile," Last updated on 18th October, 2025. Retrieved on 18th October, 2025. Available [Online]: https://www.globaldata.com/company-profile/mtn-nigeria-communications-plc/.
[20] GOtv Nigeria, "MultiChoice Africa Holdings BV," Last updated 18th October, 2025. Retrieved on 18th October, 2025. Available [Online]: https://www.gotvafrica.com/en-ng.
[21] 3GPP, "3rd Generation Partnership Project," 2024. Available [Online]: https://www.3gpp.org/.
[22] ETSI, "Evolved Universal Terrestrial Radio Access (E-UTRA); Physical channels and modulation," *ARIB STD-T104*, Release 12 (3GPP TS 36.211 V13.0.0), 2016. Available [Online]: https://id.scribd.com/document/787675839/LTE-Evolved-Universal-Terrestrial-Radio-Access-E-UTRA-Physical-channels-and-modulation-3GPP-TS-36-211-version-13-0-0-Release-13.
[23] 3GPP, "TS 23.203 - Policy and charging control architecture," *3GPP Technical Specification*, Release 13, 2016. Available [Online]: https://www.3gpp.org/DynaReport/23203.htm.
[24] 3GPP, "TS 36.300 - Evolved Universal Terrestrial Radio Access (E-UTRA) and Evolved Universal Terrestrial Radio Access Network (E-UTRAN); Overall description; Stage 2," *3GPP Technical Specification*, Release 14, 2017. Available [Online]: https://www.3gpp.org/DynaReport/36300.htm.
[25] ITU, "Frequency and network planning aspects of DVB-T2," *ITU-R Report BT.2254-2*, Dec. 2014. Available [Online]: https://www.itu.int/pub/R-REP-BT.2254-2-2014.
[26] Recommendation ITU-R P.1546-6 (08-2019), Method for Point-to-Area Predictions for Terrestrial Services in the Frequency Range 30 MHz to 4,000 MHz," P Series Radiowave Propagation, *International Telecommunication Union*, pp. 1 – 59, 2019. Available [Online]: https://www.itu.int/dms_pubrec/itu-r/rec/p/R-REC-P.1546-6-201908-I!!PDF-E.pdf.

[27] A. H. Kelechi, U. A. Samson, M. Simeon, O. Obinna, A. Alex, A. A. Aderemi, " The quality of service of the deployed LTE technology by mobile network operators in Abuja-Nigeria," *International Journal of Electrical and Computer Engineering (IJECE)*, vol. 11, no. 3, pp. 45-56, 2021. https://doi.org/10.26636/jtit.2021.151421.

[28] A. R. Ekpo, U. I. Udo, and J. O. Odim, " Characterization of LTE Parameters Relevant for Mobile Number Portability in Nigeria," *International Journal of Research in Engineering & Science*, vol. 3, no. 3, pp. 11-22, 2019. https://doi.org/10.26808/rs.re.v3i3.02.

[29] S. Hämäläinen, H. Sanneck, and C. Sartori, *LTE Self-Organising Networks (SON): Network Management Automation for Operational Efficiency*. Chichester, UK: Wiley, 2012. https://books.google.co.id/books?id=qgLs2D5Hx8AC.

[30] ETSI TS 128-313 version 16.0.0 (2020-10), "Technical Specification: 5G; Self-Organizing Networks (SON) for 5G Networks," 3GPP TS 28.313 version 16.0.0 Release 16, pp. 1 – 45. Available [Online]: https://www.etsi.org/deliver/etsi_ts/128300_128399/128313/16.00.00_60/ts_128313v160000p.pdf.

[31] J. Ramiro and K. Hamied, *Self-Organizing Networks: Self-Planning, Self-Optimization and Self-Healing for GSM, UMTS and LTE*. Chichester, UK: Wiley, 2012. https://books.google.co.id/books?id=i6Hute7zic0C.

[32] O. G. Aliu, A. Imran, M. A. Imran, and B. Evans, "A survey of self-organisation in future cellular networks," *IEEE Communications Surveys & Tutorials*, vol. 15, no. 1, pp. 336-361, 1st Quarter 2013. https://doi.org/10.1109/SURV.2012.021312.00116.

[33] M. Hata, "Empirical formula for propagation loss in land mobile radio services," *IEEE Transactions on Vehicular Technology*, vol. 29, no. 3, pp. 317-325, Aug. 1980. https://doi.org/10.1109/T-VT.1980.23859.

[34] H. Holma and A. Toskala, Eds., *LTE for UMTS: Evolution to LTE-Advanced*, 2nd ed. Chichester, UK: Wiley, 2011. https://doi.org/10.1002/9781119992943.

[35] K. I. Pedersen, F. Frederiksen, C. Rosa, H. Nguyen, L. G. U. Garcia, and Y. Wang, " An introduction to millimeter-wave mobile broadband systems," *IEEE Communications Magazine*, vol. 49, no. 6, pp. 89-95, Jun. 2011. https://doi.org/10.1109/MCOM.2011.5783993.

[36] M. Iwamura, K. Etemad, M. H. Fong, R. Nory, and R. Love, "Carrier aggregation framework in 3GPP LTE-Advanced," *IEEE Communications Magazine*, vol. 48, no. 8, pp. 60-67, Aug. 2010. https://doi.org/10.1109/MCOM.2010.5534588.

[37] R. Irmer, H. Droste, P. Marsch, M. Grieger, G. Fettweis, S. Brueck, H.-P. Mayer, L. Thiele, and V. Jungnickel, "Coordinated multipoint: Concepts, performance, and field trial results," *IEEE Communications Magazine*, vol. 49, no. 2, pp. 102-111, Feb. 2011. https://doi.org/10.1109/MCOM.2011.5706317.

[38] J. Martins, "Impact of MIMO and carrier aggregation in LTE-Advanced," M.S. thesis, Instituto Superior Técnico, Universidade de Lisboa, Lisbon, Portugal, 2013. Available [Online]: https://grow.tecnico.ulisboa.pt/wp-content/uploads/2014/10/Tese-final-Jo--o-Martins.pdf.

[39] S. N. Arinze, M. O. Alor and P. U. Okafor, "Determination of Quality of Service (QOS) in Mobile Network" *Scholars Journal of Engineering and Technology,"* vol. 6, no. 10, pp. 288-292, 2018. https://www.saspublishers.com/article/11374/download/.

[40] D. Gozálvez, D. Gómez-Barquero, D. Vargas, and N. Cardona, "Time diversity in mobile DVB-T2 systems," *IEEE Transactions on Broadcasting*, vol. 57, no. 3, pp. 617-628, Sep. 2011. https://doi.org/10.1109/TBC.2011.2161189.

[41] A. T. Ho; J.-F. Helard; Y. Nasser, "A novel combined PAPR reduction and channel estimation approach for OFDM systems," in *Proc. IEEE Int. Symp. Broadband Multimedia Systems and Broadcasting (BMSB)*, Shanghai, China, Mar. 2010, pp. 1-5. https://doi.org/10.1109/ISBMSB.2010.5463149.

[42] S. Schwarz, C. Mehlführer, and M. Rupp, "Throughput maximizing multiuser scheduling with adjustable fairness," in *Proc. IEEE Int. Conf. Communications (ICC)*, May 2011. https://doi.org/10.1109/icc.2011.5963489.

[43] H. Holma and A. Toskala, Eds., *LTE-Advanced: 3GPP Solution for IMT-Advanced*. Chichester, UK: Wiley, 2012. https://doi.org/10.1002/9781118399439.

[44] I. Viering, M. Dottling, and A. Lobinger, "A mathematical perspective of self-optimizing wireless networks," in *Proc. IEEE Int. Conf. Communications (ICC)*, Dresden, Germany, Jun. 2009, pp. 1-6. https://doi.org/10.1109/ICC.2009.5198628.

[45] C. M. Chen, C. Y. Huang, and C. Y. Chiu, " A physical cell identity self-organization algorithm in LTE-advanced systems," in *Proc. IEEE International Conference on Communications and Networking in China*, 2013. https://doi.org/10.1109/ChinaCom.2012.6417549.

[46] G. Yuan, X. Zhang, W. Wang, and Y. Yang, "Carrier aggregation for LTE-advanced mobile communication systems," *IEEE Communications Magazine*, vol. 48, no. 2, pp. 88-93, Feb. 2010. https://doi.org/10.1109/MCOM.2010.5402669.

[47] M. Chetty, S. Sundaresan, S. Muckaden, N. Feamster and E. Calandro "Measuring Broadband Performance in South Africa'' *ACM DEV-4 '13: In the Proceedings of the 4th Annual Symposium*

on Computing for Development, Article No. 1, Pages 1 – 10, 2013. https://doi.org/10.1145/2537052.2537053. ISBN: 9781450325585.

[48] DVB Project, "GOtv - DVB-T2 goes Africa," *DVB News Article*, Oct. 2011. Available [Online]: https://dvb.org/news/gotv-dvb-t2-goes-africa/.

[49] D. López-Pérez, I. Guvenc, G. de la Roche, M. Kountouris, T. Q. S. Quek, and J. Zhang, "Enhanced intercell interference coordination challenges in heterogeneous networks," *IEEE Wireless Communications*, vol. 18, no. 3, pp. 22-30, Jun. 2011. https://doi.org/10.1109/MWC.2011.5876497.

[50] M. Simsek, M. Bennis, I. Güvenç, " Enhanced intercell interference coordination in HetNets: Single vs. multiflow approach," in *Proc. IEEE IEEE Globecom Workshops (GC Wkshps)*. 2013. https://doi.org/10.1109/GLOCOMW.2013.6825074.

[51] T. S. Rappaport, S. Sun, R. Mayzus, H. Zhao, Y. Azar, K. Wang, "Millimeter wave mobile communications for 5G cellular: It will work!," *IEEE Access*, vol. 1, pp. 335-349, 2013. https://doi.org/10.1109/ACCESS.2013.2260813.

[52] IEEE Standard 802.11be-2024, "802.11be-2024 - IEEE Draft Standard for Information technology--Telecommunications and information exchange between systems Local and metropolitan area networks--Specific requirements - Part 11: Wireless LAN Medium Access Control (MAC) and Physical Layer (PHY) Specifications Amendment: Enhancements for Extremely High Throughput (EHT)," *IEEE 35.110 - Networking*, 2023. Available [Online]: https://ieeexplore.ieee.org/document/10058126.

[53] The MathWorks Inc., "MATLAB® and Simulink® Release 2025a," Natick, MA, USA, 2025. Available [Online]: www.mathworks.com.

[54] H. Minn, M. Zeng, and V. K. Bhargava, "On timing offset estimation for OFDM systems," *IEEE Communications Letters*, vol. 4, no. 7, pp. 242-244, Jul. 2000. https://doi.org/10.1109/4234.852929.

[55] V. A. Akpan, "Model-based embedded-processor systems design methodologies: Modeling, syntheses, implementation and validation," *African Journal of Computing and ICTs*, vol. 5, no. 1, pp. 1-26, Mar. 2012. Available [Online]: https://africanjournalofcomputingict1.wordpress.com/wp-content/uploads/2017/08/vol-5-no-1-january-20121.pdf.

[56] V. A. Akpan, "An FPGA realization of integrated embedded multi-processors system: A hardware-software co-design approach," *Journal of Advanced Research in Embedded System (JoARES)*, vol. 2, no. 1, pp. 1-27, Jan. 2015.

[57] V. A. Akpan, "FPGA-in-the-Loop implementation of an adaptive matrix inversion algorithmic co-processor: A dual-processor system design," *Journal of Advanced Research in Embedded System (JoARES)*, vol. 2, no. 1, pp. 28-63, Jan. 2015.

[58] V. A. Akpan, "Hard and soft embedded FPGA processor systems design: Design considerations and performance comparisons," *International Journal of Engineering and Technology*, vol. 3, no. 11, pp. 1000-1020, Nov. 2013. Available [Online]: https://id.scribd.com/document/401430795/16-HardandSoftEmbeddedFPGAProcessorSystemsDesign-pdf.

[59] V. A. Akpan, D. Chasapis, and G. D. Hassapis, "FPGA implementation of neural network-based AGPC for nonlinear F-16 aircraft auto-pilot control: Part 1 - Modeling, synthesis, verification and FPGA-in-the-loop co-sim," *American Journal of Embedded Systems and Applications*, vol. 9, no. 1, pp. 6-36, Jun. 2022. https://www.sciencepublishinggroup.com/article/10.11648/10068476.

[60] V. A. Akpan, D. Chasapis, and G. D. Hassapis, "FPGA implementation of neural network-based AGPC for nonlinear F-16 aircraft auto-pilot control: Part 2 - Implementation of embedded PowerPC™440 with AGPC," *American Journal of Embedded Systems and Applications*, vol. 9, no. 2, pp. 37-65, Dec. 2022. https://www.sciencepublishinggroup.com/article/10.11648/j.ajesa.20220902.11.

[61] M. Renfors, J. Yli-Kaakinen, T. Levanen, M. Valkama, "Fast-convolution filtered OFDM waveforms with adjustable CP length," in *Proc. IEEE Global Conference on Signal and Information Processing (GlobalSIP)*, Washington, DC, USA, Dec. 2016. https://doi.org/10.1109/GlobalSIP.2016.7905919.

[62] Z. E. Ankarali, B. Peköz, and H. Arslan, "Flexible radio access beyond 5G: A future projection on waveform, numerology, and frame design principles," *IEEE Access*, vol. 5, pp. 18295-18309, 2017. https://doi.org/10.1109/ACCESS.2017.2684783.

[63] M. Krstic, E. Grass, F. K. Gürkaynak, and P. Vivet, "Globally asynchronous, locally synchronous circuits: Overview and outlook," *IEEE Design & Test of Computers*, vol. 24, no. 5, pp. 430-441, Sep.-Oct. 2007. https://doi.org/10.1109/MDT.2007.164.

[64] T. M. Schmidl and D. C. Cox, "Robust frequency and timing synchronization for OFDM," *IEEE Transactions on Communications*, vol. 45, no. 12, pp. 1613-1621, Dec. 1997. https://doi.org/10.1109/26.650240.

[65] R. Woods, J. McAllister, G. Lightbody, and Y. Yi, *FPGA-based Implementation of Signal Processing Systems*, 2nd ed. Chichester, UK: Wiley, 2017. https://books.google.co.id/books?id=O2-RPrJUHJAC.

[66] C. Dick, F. Harris, and M. Rice, "FPGA implementation of carrier synchronization for QAM receivers," *Journal of VLSI Signal Processing Systems for Signal, Image and Video Technology*, vol. 36, no. 1, pp. 57-71, Jan. 2004. https://doi.org/10.1023/B:VLSI.0000008070.30837.e1.

[67] A. M. Wyglinski, F. Labeau, and P. Kabal, "Bit loading with BER-constraint for multicarrier systems," *IEEE Transactions on Wireless Communications*, vol. 4, no. 4, pp. 1383-1387, Jul. 2005. https://doi.org/10.1109/TWC.2005.850313.

[68] B. Khan, D.D. Kleiner, D. Talmage, "OPTIPRISM: a distributed hierarchical network management system for all-optical networks," in *Proc. IEEE Global Telecommunications Conference (Cat. No.01CH37270)*, San Antonio, TX, USA, Nov. 2001, pp. 1827–1831. https://doi.org/10.1109/GLOCOM.2001.965837.

[69] L. Vangelista, N. Benvenuto, and S. Tomasin, "Key technologies for next-generation terrestrial digital television standard DVB-T2," *IEEE Communication Magazine*, vol. 47, no. 10, pp. 146–153, Oct. 2009. https://doi.org/10.1109/MCOM.2009.5273822.

[70] Y. Wu and W. Y. Zou, "Orthogonal frequency division multiplexing: A multi-carrier modulation scheme," *IEEE Transactions on Consumer Electronics*, vol. 41, no. 3, pp. 392–399, Aug. 1995. https://doi.org/10.1109/30.468055.

[71] J. Armstrong, "OFDM for optical communications," *J. Lightw. Technol.*, vol. 27, no. 3, pp. 189–204, Feb. 2009. https://doi.org/10.1109/JLT.2008.2010061.

[72] T. S. Rappaport, *Wireless Communications: Principles and Practice*, 2nd ed., Upper Saddle River, NJ, USA: Prentice Hall, 2002. https://link.gale.com/apps/doc/A97115718/AONE?u=anon~322e4e18&sid=google-Scholar&xid=acb10fd4.

[73] C. Hellge, D. Gómez-Barquero, T. Schierl, and T. Wiegand, "Layer-aware forward error correction for mobile broadcast of layered media," *IEEE Trans. Multimedia*, vol. 13, no. 3, pp. 551–562, Jun. 2011. https://doi.org/10.1109/TMM.2011.2129499.

[74] C. Berrou, A. Glavieux, and P. Thitimajshima, "Near Shannon limit error-correcting coding and decoding: Turbo-codes. 1," In the *Proceedings of the 1993 IEEE International Conference on Communication* (ICC), Geneva, Switzerland, May 1993, pp. 1064–1070. https://doi.org/10.1109/ICC.1993.397441.

[75] S. H. Han and J. H. Lee, "An overview of peak-to-average power ratio reduction techniques for multicarrier transmission," *IEEE Wireless Commun.*, vol. 12, no. 2, pp. 56–65, Apr. 2005. https://doi.org/10.1109/MWC.2005.1421929.

[76] H. Ochiai and H. Imai, "On the distribution of the peak-to-average power ratio in OFDM signals," *IEEE Trans. Commun.*, vol. 49, no. 2, pp. 282–289, Feb. 2001. https://doi.org/10.1109/26.905885.

[77] T. Jiang and Y. Wu, "An overview: Peak-to-average power ratio reduction techniques for OFDM signals," *IEEE Trans. Broadcast.*, vol. 54, no. 2, pp. 257–268, Jun. 2008. https://doi.org/10.1109/TBC.2008.915770.

[78] R. van Nee and R. Prasad, *OFDM for Wireless Multimedia Communications*. Boston, MA, USA: Artech House, 2000. https://dl.acm.org/doi/abs/10.5555/555664.

[79] J. A. C. Bingham, "Multicarrier modulation for data transmission: An idea whose time has come," *IEEE Communications Magazine*, vol. 28, no. 5, pp. 5–14, May 1990. https://doi.org/10.1109/35.54342.

[80] P. Viland, G. Zaharia and J. F. Helard, "Improved Balanced 2n-PSK STTCs for Any Number of Transmit Antennas from a New and General Design Method," *VTC Spring 2009 - IEEE 69th Vehicular Technology Conference*, Barcelona, Spain, 2009, pp. 1-5, https://doi.org/10.1109/VETECS.2009.5073590.

[81] G. L. Stüber, *Principles of Mobile Communication*, 4rd ed., New York, NY, USA: Springer, 2017. Available [Online]: https://books.google.co.id/books?id=cSYmDwAAQBAJ.

[82] J. G. Proakis and M. Salehi, *Digital Communications*, 5th ed. New York, NY, USA: McGraw-Hill, 2008. [Online]. Available: https://thuvienso.tnut.edu.vn/handle/123456789/997.

[83] Y. Li, "Simplified channel estimation for OFDM systems with multiple transmit antennas," *IEEE Trans. Wireless Commun.*, vol. 1, no. 1, pp. 67–75, Jan. 2002. https://doi.org/10.1109/7693.975446.

[84] D. K. Barton, *Radar System Analysis and Modeling*. Norwood, MA, USA: Artech House, 2005. Available [Online]: https://books.google.co.id/books?id=dvlPAwAAQBAJ.

[85] Nigerian Communications Commission (NCC), "National frequency allocation table," *NCC Official Document*, Lagos, Nigeria, 2021. Available [Online]: https://ncc.gov.ng/industry/spectrum-administration/frequency-allocation-tables.

[86] M. C. Davey and D. MacKay, "Low-density parity check codes over GF(q)," *Information Theory Workshop (Cat. No.98EX131)*, Killarney, Ireland, Jun. 1998. https://doi.org/10.1109/ITW.1998.706440.

[87] G. Plumb, "DVB-T2: An Update from the UK Rollout," British Broadcasting Corporation, United Kingdom, pp. 1 – 23, March, 2009. Available [Online]: https://downloads.bbc.co.uk/rd/pubs/presentations/pdffiles/t2-dvb-world-gp-03-09-ppt.pdf.

[88] R. A. Shafik, M. S. Rahman, and A. R. Islam, "On the extended relationships among EVM, BER and SNR as performance metrics," *In the Proceedings of the International Conference on Electrical and Computer Engineering* (ICECE), Dhaka, Bangladesh, Dec. 2006. https://doi.org/10.1109/ICECE.2006.355657.

[89] J. W. Yin, G. J. Zhu, X. Han, W. Ge, L. Li and Y. N. Tian, Iterative Channel Estimation-Based Soft Successive Interference Cancellation for Multiuser Underwater Acoustic Communication, *The Journal of the Acoustical Society of America*, vol. 150, pp. 133 – 144, 2021. https://doi.org/10.1121/10.0005476.

[90] M. M. Buddhikot, "Understanding dynamic spectrum access: Models, taxonomy and challenges," in *Proc. IEEE Int. Symp. New Frontiers in Dynamic Spectrum Access Networks (DySPAN)*, Dublin, Ireland, Apr. 2007, pp. 649-663. https://doi.org/10.1109/DYSPAN.2007.88.

[91] E. Lechman and M. Popowska ''Harnessing digital technologies for poverty reduction. Evidence for low-income and lower-middle income countries," *Telecommunications Policy*, vol. 46 Issues 6, July 2022, 102313. https://doi.org/10.1016/j.telpol.2022.102313.

[92] V. A. Akpan, E. C. Njoku, and E. I. Obi, "Slice-specific machine learning models for intrusion detection in 5G telecommunication networks," *International Journal of Wireless Communication and Mobile Computing*, vol. 12, no. 2, pp. 93 – 118, 2025. https://doi.org/10.11648/j.wcmc.20251202.14.

[93] C. Zhang, P. Patras, and H. Haddadi, "Deep learning in mobile and wireless networking: A survey," *IEEE Communications Surveys & Tutorials*, vol. 21, no. 3, pp. 2224-2287, 3rd Quarter 2019. https://doi.org/10.1109/COMST.2019.2904897.

[94] N. C. Luong, D. T. Hoang, S. Gong, D. Niyato, P. Wang, Y.-C. Liang, " Applications of Deep Reinforcement Learning in Communications and Networking: A Survey," *IEEE Communications Surveys & Tutorials*, vol. 21, no. 4, pp. 3133-3174, 4th Quarter 2019. https://doi.org/10.1109/COMST.2019.2916583.

[95] R. Li, Z. Zhao, X. Zhou, G. Ding, Y. Chen, Z. Wang, "Intelligent 5G: When cellular networks meet artificial intelligence," *IEEE Wireless Communications*, vol. 24, no. 5, pp. 175-183, Oct. 2017. https://doi.org/10.1109/MWC.2017.1600304WC.

[96] A. Garcia Saavedra and X. Costa-Pérez, "O-RAN: Disrupting the virtualized RAN ecosystem," *IEEE Communications Standards Magazine*, vol. 5, no. 4, pp. 96-103, Dec. 2021. https://doi.org/10.1109/MCOMSTD.101.2000014.

[97] K. Norrman, M. Näslund, and E. Dubrova, "Protecting IMSI and user privacy in 5G networks," in *Proc. of the 9th EAI International Conference on Mobile Multimedia Communications*, 2016, pp. 159-166. https://dl.acm.org/doi/abs/10.5555/3021385.3021415.

[98] A. Shaik, R. Borgaonkar, N. Asokan, V. Niemi, and J.-P. Seifert, "Practical attacks against privacy and availability in 4G/LTE mobile communication systems," *arXiv preprint arXiv:1510.07563*, 2015. https://doi.org/10.48550/arXiv.1510.07563.

[99] G. Auer, V. Giannini, C. Desset, I. Godor, P. Skillermark, M. Olsson, M. A. Imran, D. Sabella, M. J. Gonzalez, O. Blume, and A. Fehske, "How much energy is needed to run a wireless network?," *IEEE Wireless Communications*, vol. 18, no. 5, pp. 40-49, Oct. 2011. https://doi.org/10.1109/MWC.2011.6056691.